RSC Advances

ROYAL SOCIETY OF CHEMISTRY

PAPER

View Article Online
View Journal | View Issue



Cite this: *RSC Adv.*, 2024, **14**, 5907

# New pyrazolylindolin-2-one based coumarin derivatives as anti-melanoma agents: design, synthesis, dual BRAF$^{V600E}$/VEGFR-2 inhibition, and computational studies†

Ahmed Sabt, [a] Mohammed A. Khedr, [bc] Wagdy M. Eldehna, [d] Abdelsamed I. Elshamy, [a] Mohamed F. Abdelhameed, [e] Rasha M. Allam [e] and Rasha Z. Batran *[a]

Malignant melanoma is the most invasive skin cancer with the highest risk of death. The inhibition of BRAF$^{V600E}$ appears relevant for overcoming secondary resistance developed during melanoma treatment. BRAF$^{V600E}$ triggers angiogenesis *via* modification of the expression of angiogenic inducers, which play a crucial role in the metastasis of melanoma. Accordingly, the dual inhibition of the BRAF$^{V600E}$/VEGFR-2 signaling pathway is considered a rational approach in the design of anti-melanoma candidates. In this study, a new class of pyrazolylindolin-2-one linked coumarin derivatives as dual BRAF$^{V600E}$/VEGFR-2 inhibitors targeting A375 melanoma cells was designed. Target compounds were tailored to occupy the pockets of BRAF$^{V600E}$ and VEGFR-2. Most of the synthesized compounds demonstrated potent mean growth inhibitory activity against A375 cells. Compound **4j** was the most active cytotoxic derivative, displaying an $IC_{50}$ value at a low micromolar concentration of 0.96 μM with a significant safety profile. Moreover, **4j** showed dual potent inhibitory activity against BRAF$^{V600E}$ and VEGFR-2 ($IC_{50}$ = 1.033 and 0.64 μM, respectively) and was more active than the reference drug sorafenib. Furthermore, derivative **4j** caused significant G0/G1 cell cycle arrest, induced apoptosis, and inhibited the migration of melanoma cells. Molecular docking showed that compound **4j** achieved the highest Δ*G* value of −9.5 kcal mol$^{-1}$ against BRAF$^{V600E}$ and significant Δ*G* of −8.47 kcal mol$^{-1}$ against VEGFR-2. Furthermore, the structure–activity relationship study revealed that TPSA directly contributed to the anticancer activity of the tested compounds.

Received 6th January 2024
Accepted 29th January 2024

DOI: 10.1039/d4ra00157e

rsc.li/rsc-advances



## 1. Introduction

Melanoma is one of the most aggressive forms of skin malignancy and considered the leading cause of death among other skin cancers.[1–3] Dysregulation of the RAS-RAF-MEK-ERK cascade, a mitogen-activated protein kinase (MAPK) pathway, is a critical step in melanoma pathogenesis.[4]

RAF family proteins involve serine–threonine kinases composed of A-RAF, B-RAF, and C-RAF, which regulate intracellular signal transduction. Among them, the BRAF oncogene shows better biochemical potencies than A-RAF and C-RAF isoforms owing to its higher basal kinase activity and ease of activation by RAS, which explains the observed frequent mutational activation of the BRAF gene in human tumors.[5–7] Approximately 90% of the detected BRAF mutations in human cancer are amino acid substitution at the nucleotide residue 600 (V600E) of valine by glutamic acid.[8] The BRAF$^{V600E}$ mutation leads to constitutive kinase activation, which is 500–700-fold greater than wild-type BRAF, resulting in the amplification of the MAPK signaling pathway and stimulation of vascular endothelial growth factor (VEGF), thus inducing metastasis.[9,10] This mutation is mostly associated with melanoma.[11–13]

The successful inhibition of BRAF was a turning point in the development of anti-melanoma agents. Targeted therapy with BRAF inhibitors represents a milestone in the treatment of metastatic melanoma that harbors BRAF$^{V600E}$ mutations. However, resistance to the treatment was identified in patients

[a]*Chemistry of Natural Compounds Department, Pharmaceutical and Drug Industries Research Institute, National Research Centre, Dokki, Cairo, 12622, Egypt. E-mail: rasha_batran@yahoo.com*

[b]*Department of Pharmaceutical Chemistry, College of Pharmacy, Kuwait University, Safat 13110, Kuwait*

[c]*Department of Pharmaceutical Chemistry, Faculty of Pharmacy, Helwan University, 11795, Egypt*

[d]*Department of Pharmaceutical Chemistry, Faculty of Pharmacy, Kafrelsheikh University, Kafrelsheikh, 33516, Egypt*

[e]*Pharmacology Department, Medical and Clinical Research Institute, National Research Centre, Dokki, Cairo 12622, Egypt*

† Electronic supplementary information (ESI) available. See DOI: https://doi.org/10.1039/d4ra00157e

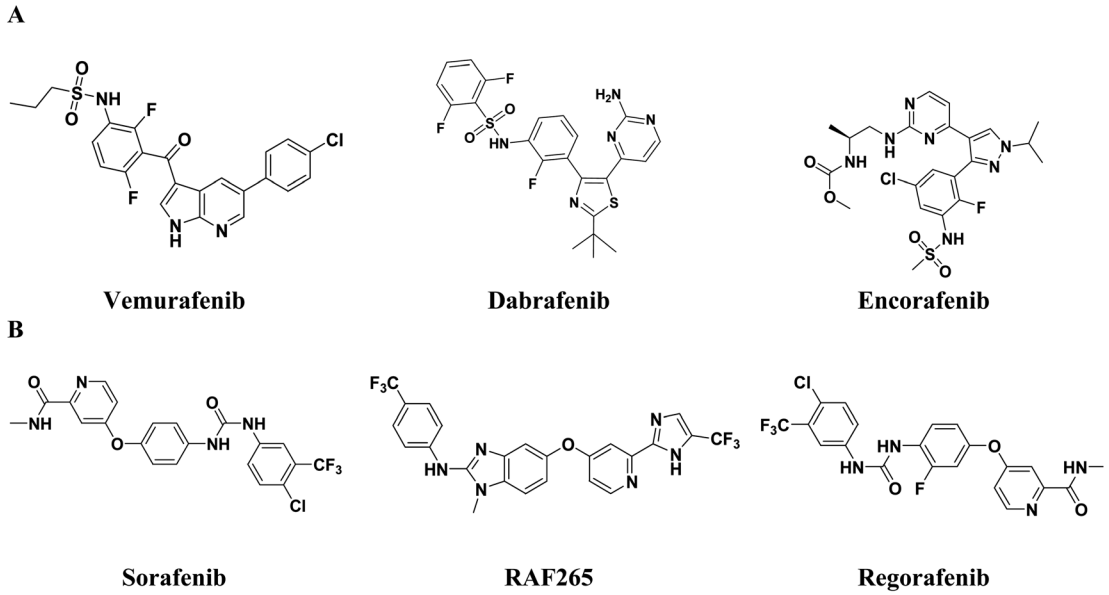


Fig. 1 (A) Examples of FDA approved anti-melanoma drugs. (B) Dual inhibitors of BRAF/VEGFR-2.

receiving these drugs within months, which makes the discovery of new targeted anti-melanoma therapeutics that can selectively block tumor signals in the RAS-RAF-MAPK complex network a substantial therapeutic challenge.[14–16]

Various drug development programs have been initiated, such as the dual inhibition of $BRAF^{V600E}$ and VEGFR-2, which has been considered a rational approach in the design of anti-melanoma candidates.[17,18] This approach aims to seek alternative chemical backbones that avoid the resistance and side effects acquired by current anti-melanoma FDA approved therapies such as vemurafenib,[19] dabrafenib,[20] and encorafenib,[21] which may be due to paradoxical MAPK activation in cells expressing wild-type BRAF.[22–25] Dual inhibitors such as sorafenib and RAF265, which are type II inhibitors, were approved for or entered clinical trials (Fig. 1).[26,27] Sorafenib, *i.e.*, BAY 43e9006, is a multi-kinase inhibitor with dual inhibitory properties against VEGFR and RAF kinases. It suppresses MAPK signaling *via* RAF inhibition in various cancer cell lines including melanoma.[28] Regorafenib, *i.e.*, BAY 73-4506, effectively inhibits a wide range of angiogenic kinases such as VEGFR-1/2/3 and intracellular signaling kinases, including BRAF and CRAF.[29] Furthermore, RAF265 is a strong dual RAF/VEGFR-2 inhibitor that efficiently suppresses the growth and survival of cancer cells by blocking tumor development and preventing blood supply to cancerous cells (Fig. 1).[30]

Coumarin derivatives are known for their potent anticancer activity, displaying remarkable activity against human malignant melanoma and preventing its recurrence.[31–33] Moreover, coumarin analogues exhibit selective RAF inhibiting efficacies, making the coumarin nucleus a prominent bioactive structural motif in the search for new anti-melanoma cancer molecules.[34,35] Furthermore, 4-hydoxycoumarin derivatives have been extensively used as a valuable core in the synthesis of VEGFR-2 inhibitors.[36,37] Moreover, several FDA approved drugs and inhibitors in clinical trials containing pyrazole (*e.g.*, encorafenib and GDC0879) and indole or indole isosteres (*e.g.*, vemurafenib (azaindole), SB-590885 (indene) and XL281(indole)[38]) have been investigated for potent and selective anti-BRAF activity. Alternatively, pyrazole and indole derivatives have also been reported for their potent VEGFR-2 inhibitory activity (Fig. 1 and 2).[30–43]

In this work, we aim to discover dual $BRAF^{V600E}$ and VEGFR-2 inhibitors that were rationally designed based on the ABC triaryl pyrazole system,[44–46] simultaneously displaying the pharmacophoric features of $BRAF^{V600E}$ and VEGFR-2 inhibitors (Fig. 2). Based on the above-mentioned studies, a new series of pyrazolyl indoline-based coumarin derivatives was designed, synthesized, and biologically assessed for their cytotoxic activity against melanoma cells. Furthermore, the promising derivatives were evaluated for dual inhibition towards $BRAF^{V600E}$ and VEGFR-2, cell migration, cell cycle analysis and apoptosis. The molecular modeling study was carried out to investigate the binding mode of the promising candidates in the binding pockets of $BRAF^{V600E}$ and VEGFR-2.

## 2. Results and discussion

### 2.1. Chemistry

The synthetic procedures for the synthesis of the target pyrazolylindoline-2-one-coumarin hybrids **4a–j**, **5a–j** and **6a–j** are demonstrated in Scheme 1. Intermediate chalcone derivatives **2a–c** were prepared through the Claisen–Schmidt condensation reaction of 3-acetyl-4-hydroxycoumarin **1** and the appropriate aromatic aldehydes, namely, 4-fluorobenzaldehyde, 4-chlorobenzaldehyde and/or 4-bromobenzaldehyde according to the reported procedures.[47,48] The cyclo–addition reaction of hydrazine hydrate with chalcone intermediates **2a–c** furnished the corresponding pyrazolines **3a–c**, respectively. The target

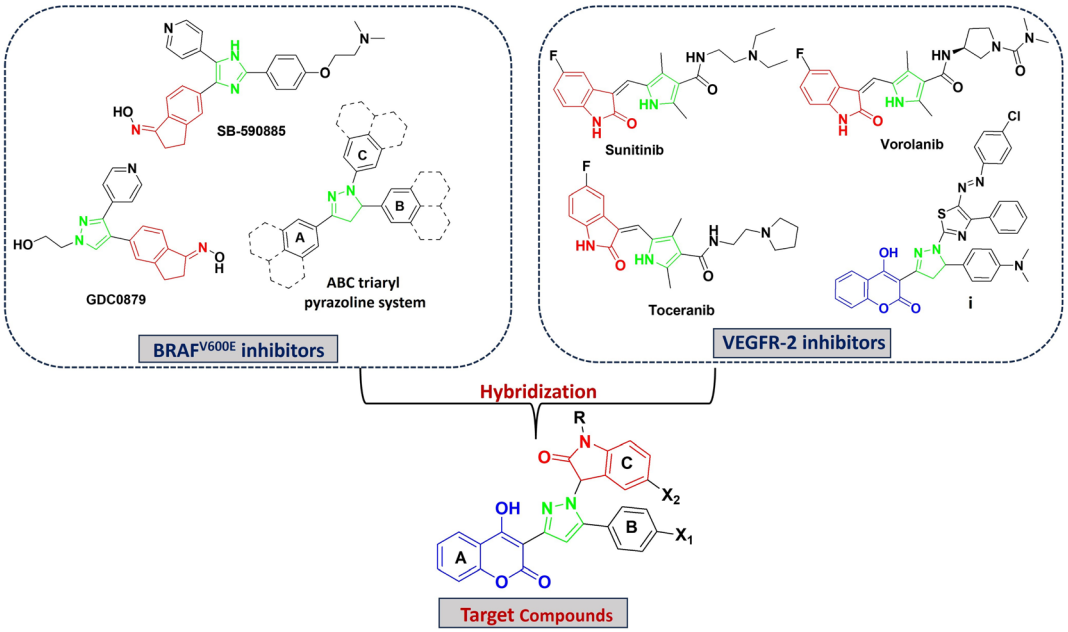


Fig. 2 Rationale for the design of target compounds.

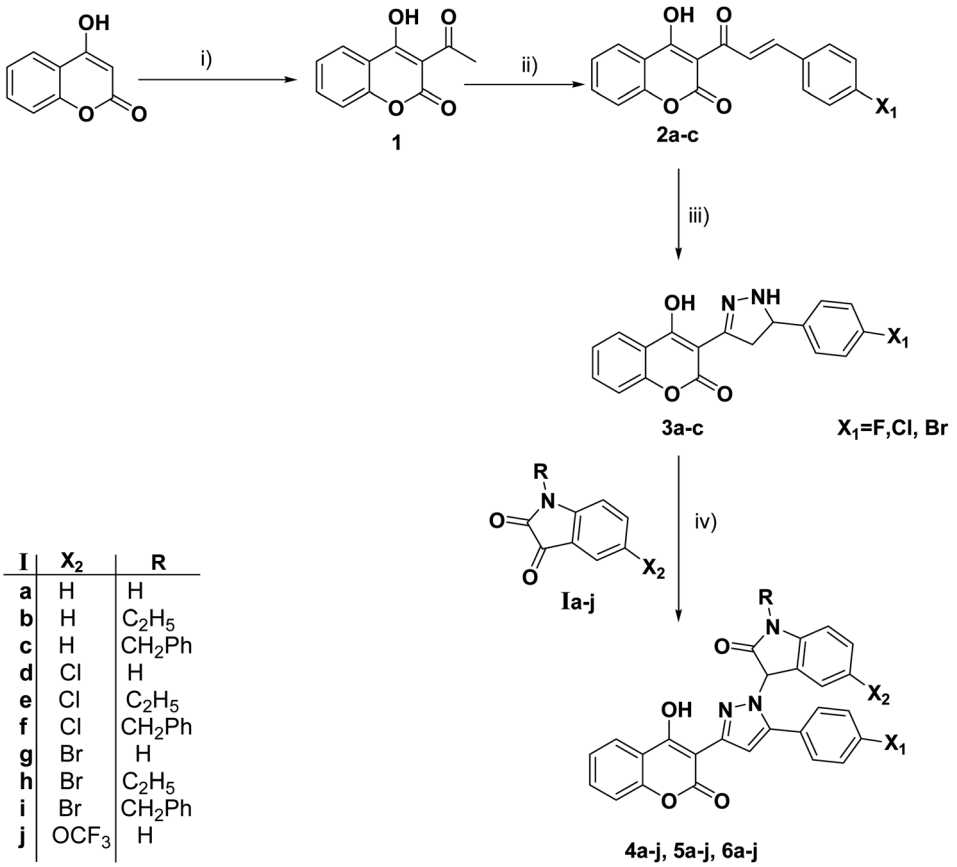


| I | $X_2$ | R |
|---|---|---|
| a | H | H |
| b | H | $C_2H_5$ |
| c | H | $CH_2Ph$ |
| d | Cl | H |
| e | Cl | $C_2H_5$ |
| f | Cl | $CH_2Ph$ |
| g | Br | H |
| h | Br | $C_2H_5$ |
| i | Br | $CH_2Ph$ |
| j | $OCF_3$ | H |

Scheme 1 Reagents and conditions: (i) $POCl_3$/AcOH/reflux. (ii) ArCHO/piperidine/EtOH/reflux. (iii) $NH_2NH_2 \cdot H_2O$/EtOH/reflux. (vi) Isatin derivatives/EtOH/reflux.

pyrazolylindolin-2-one derivatives **4a–j**, **5a–j** and **6a–j** were afforded by reacting pyrazoline compounds **3a–c** with isatin derivatives *via* the elimination of a water molecule (Scheme 1). The structures of the newly synthesized compounds were assigned *via* elemental and spectral analyses including $^{1}$H NMR and $^{13}$C NMR.

### 2.2. Biology

**2.2.1. *In vitro* cytotoxic effect of synthesized compounds against melanoma cells A375.** The target compounds **4a–j**, **5a–j** and **6a–j** were assessed for their *in vitro* cytotoxic activity against the A375 human melanoma cell line *via* SRB assay using sorafenib as a positive control. The cytotoxic effects were expressed by median growth inhibitory concentration ($IC_{50}$), as shown in Table 1. The results revealed that among the derivatives, **4j**, **4f**, **4i**, **5f** and **5i** were the most potent compounds with $IC_{50}$ values of 0.96, 1.114, 1.28, 1.09 and 1.02 μM, respectively, displaying higher cytotoxic activity than sorafenib and showing a significant safety profile, as presented in Table 2. Regarding the other compounds, most of them exerted promising cytotoxic activity against melanoma cells with $IC_{50}$ values of <10 μM, ranging from 8.99 μM (**6e**) to 3.8 μM (**5c**), while five derivatives, **4b**, **4e**, **4h**, **5b**, and **6h**, exhibited weak cytotoxic activity with $IC_{50}$ values of 79.47, 82.63, 38.65, 33.76 and 47.22 μM, respectively.

Table 1 Cytotoxic activity of the target compounds on A375 cells *via* the SRB assay[a]

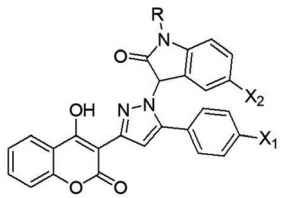

**4a-j, 5a-j, 6a-j**

| Compound | R | $X_1$ | $X_2$ | ($IC_{50}$, μM) |
|---|---|---|---|---|
| **4a** | H | F | H | 6.25 ± 0.75 |
| **4b** | $CH_2CH_3$ | F | H | 79.47 ± 3.60 |
| **4c** | $CH_2PH$ | F | H | 4.6 ± 0.32 |
| **4d** | H | F | Cl | 4.3 ± 0.38 |
| **4e** | $CH_2CH_3$ | F | Cl | 82.63 ± 2.65 |
| **4f** | $CH_2Ph$ | F | Cl | 1.114 ± 0.02 |
| **4g** | H | F | Br | 5.85 ± 0.95 |
| **4h** | $CH_2CH_3$ | F | Br | 38.65 ± 2.60 |
| **4i** | $CH_2Ph$ | F | Br | 1.28 ± 0.02 |
| **4j** | H | F | $OCF_3$ | 0.96 ± 0.03 |
| **5a** | H | Cl | H | 7.13 ± 0.44 |
| **5b** | $CH_2CH_3$ | Cl | H | 33.76 ± 1.80 |
| **5c** | $CH_2Ph$ | Cl | H | 3.8 ± 0.22 |
| **5d** | H | Cl | Cl | 5.43 ± 0.82 |
| **5e** | $CH_2CH_3$ | Cl | Cl | 7.32 ± 0.69 |
| **5f** | $CH_2Ph$ | Cl | Cl | 1.09 ± 0.09 |
| **5g** | H | Cl | Br | 6.18 ± 0.73 |
| **5h** | $CH_2CH_3$ | Cl | Br | 5.44 ± 0.41 |
| **5i** | $CH_2Ph$ | Cl | Br | 1.02 ± 0.07 |
| **5j** | H | Cl | $OCF_3$ | 4.17 ± 0.36 |
| **6a** | H | Br | H | 8.45 ± 0.60 |
| **6b** | $CH_2CH_3$ | Br | H | 68.38 ± 3.50 |
| **6c** | $CH_2Ph$ | Br | H | 4.84 ± 0.30 |
| **6d** | H | Br | Cl | 6.25 ± 0.72 |
| **6e** | $CH_2CH_3$ | Br | Cl | 8.99 ± 0.78 |
| **6f** | $CH_2Ph$ | Br | Cl | 4.36 ± 0.22 |
| **6g** | H | Br | Br | 7.32 ± 0.80 |
| **6h** | $CH_2CH_3$ | Br | Br | 47.22 ± 1.90 |
| **6i** | $CH_2Ph$ | Br | Br | 5.47 ± 0.20 |
| **6j** | H | Br | OCF3 | 4.37 ± 0.24 |
| **Sorafenib** | — | — | — | 3.2 ± 0.67 |

[a] The cytotoxic activity was determined after treatment of A375 with serial dilution of the target compounds for 72 h, where data are expressed as mean ± SD ($n = 3$).

The cancerous specificity and the safety of the most active derivatives were evaluated on normal human skin fibroblast cells (HSF) and their selectivity index values were calculated and shown in Table 2. The five most potent derivatives (**4j**, **4f**, **5i**, **5f** and **4i**) showed relatively low toxicity with $IC_{50}$ values on HSF cells of 9.58, 4.18, 3.63, 3.59 and 3.26 μM, respectively. Among them, compound **4j** was the safest hybrid (SI = 9.9), displaying the highest selectivity and potency towards melanoma cells A375.

**2.2.2. *In vitro* $BRAF^{V600E}$ and VEGFR-2 inhibitory activity of compound 4j.** The most promising derivative **4j**, which showed the most potent activity against A375 melanoma cells and the highest SI, was further evaluated for its inhibitory effect on both $BRAF^{V600E}$ and VEGFR-2 kinases in A375 cells compared to sorafenib (Table 3). The results of the $BRAF^{V600E}$ inhibition assay showed the pronounced inhibitory activity of **4j** ($IC_{50}$ = 1.033 μM), which was 2-fold more active than the reference sorafenib ($IC_{50}$ = 2.86 μM). The selected derivative exhibited significant inhibition activity against VEGFR-2 with an $IC_{50}$ value of 0.64 μM *versus* 1.94 μM for sorafenib. These results are consistent with the cytotoxic effect of compound **4j** against A375 cells, highlighting the postulation that $BRAF^{V600E}$ and VEGFR-2 inhibition can be the molecular mechanisms of the potential cytotoxic effect of **4j**, especially given that inhibitors of $BRAF^{V600E}$ kinase have been reported to be antiproliferative agents against melanoma.[49] Therefore, **4j** was selected for the following tests.

**2.2.3. Effect of 4j on the cell cycle distribution in melanoma cells.** The cell cycle distribution using DNA flow cytometry was used to assess the observed growth inhibition after treatment of the A375 cell line with **4j** and sorafenib (Fig. 3). Treatment with **4j** resulted in major changes in all cell cycle phases

Table 2 $IC_{50}$ values (μM) of the most active compounds on melanoma A375 and HSF cell lines and the selectivity index

| Compound | A375 $IC_{50}$ (μM) | HSF $IC_{50}$ (μM) | Selectivity index (SI) |
|---|---|---|---|
| **4f** | 1.114 ± 0.02 | 4.18 ± 0.25 | 3.6 |
| **4i** | 1.28 ± 0.021 | 3.26 ± 0.29 | 2.5 |
| **4j** | 0.96 ± 0.03 | 9.58 ± 0.73 | 9.9 |
| **5f** | 1.09 ± 0.09 | 3.59 ± 0.32 | 3.3 |
| **5i** | 1.02 ± 0.07 | 3.63 ± 0.76 | 3.5 |

Table 3 *In vitro* $BRAF^{V600E}$ and VEGFR-2 inhibitory activities

| Compound | $BRAF^{V600E}$ ($IC_{50}$, μM) | VEGFR-2 ($IC_{50}$, μM) |
|---|---|---|
| **4j** | 1.03 ± 0.71 | 0.64 ± 0.08 |
| **Sorafenib** | 2.86 ± 0.45 | 1.94 ± 0.05 |

compared to control cells. Compound **4j** caused a significant increase ($P < 0.05$) in the cell population of the G0/G1-phase (the non-proliferating cell proportion) from 55.71% to 74.14% compared to the control cells, indicating cell cycle arrest and implying that G0/G1 cell cycle arrest is a fundamental mechanism of the anticancer activities of coumarin derivatives, as previously reported.[50] Reciprocally, treatment with **4j** showed a meaningful decrease in the cell percentage of the S phase (the DNA synthesis phase) after 48 h treatment from 17.62% to 9.86% concomitantly with a decrease in the cell percentage in the G2/M phase from 26.67% to 16.00% (Fig. 3A and B), respectively. Also, no significant changes were observed in the pre-G phase after treatment with **4j** from 1.21% to 1.88% compared with the control cells.

Treatment with sorafenib resulted in observable cell cycle arrest at the G0/G1 phase from 55.71% to 60.43%, with almost the same alterations in the S phase from 17.62% to 16.55% and G2/M phase from 26.67% to 23.02% compared to the control cells (Fig. 3A and B), respectively. However, treatment with sorafenib resulted in significant cell death ($P < 0.05$) manifested by a considerable increase in the cell population of the Pre-G phase from 1.21% to 22.88% compared with the control cells (Fig. 3C). These results are consistent with that reported for sorafenib, which significantly inhibits the growth of cancer cells through the accumulation of cells in the pre-G1 phase.[51]

These findings shed light on the mode of action of coumarin derivatives as antiproliferative agents (inducing G0/G1 arrest), which differs from the cytotoxic effect of sorafenib (inducing pre-G1 arrest) and highlight the potential use of coumarins as effective anticancer agents in melanoma treatment. This can be explained by the fact that the G1 phase is a phase that precedes DNA replication, in which the cellular conditions influence cell cycle progression, causing DNA to either rebuild in a cell or initiate apoptosis, and several studies address the role of G0/G1 phase arrest in intensifying cellular apoptosis.[52]

**2.2.4. Modes of cell death in melanoma cells.** To determine the exact mechanism of cell death (apoptosis/necrosis) induced by **4j** and sorafenib, the treated A375 cells were evaluated using Annexin-V/FITC staining coupled with flow cytometry. The results are highlighted in Fig. 4A and B, showing the variations in apoptosis and necrosis detection between the groups.

Compound **4j** induced significant ($p < 0.05$) total cell death of A375 cells (nearly 10.22%) by mainly apoptotic death with early apoptosis of 6.07% and late apoptosis of 2.3% compared with

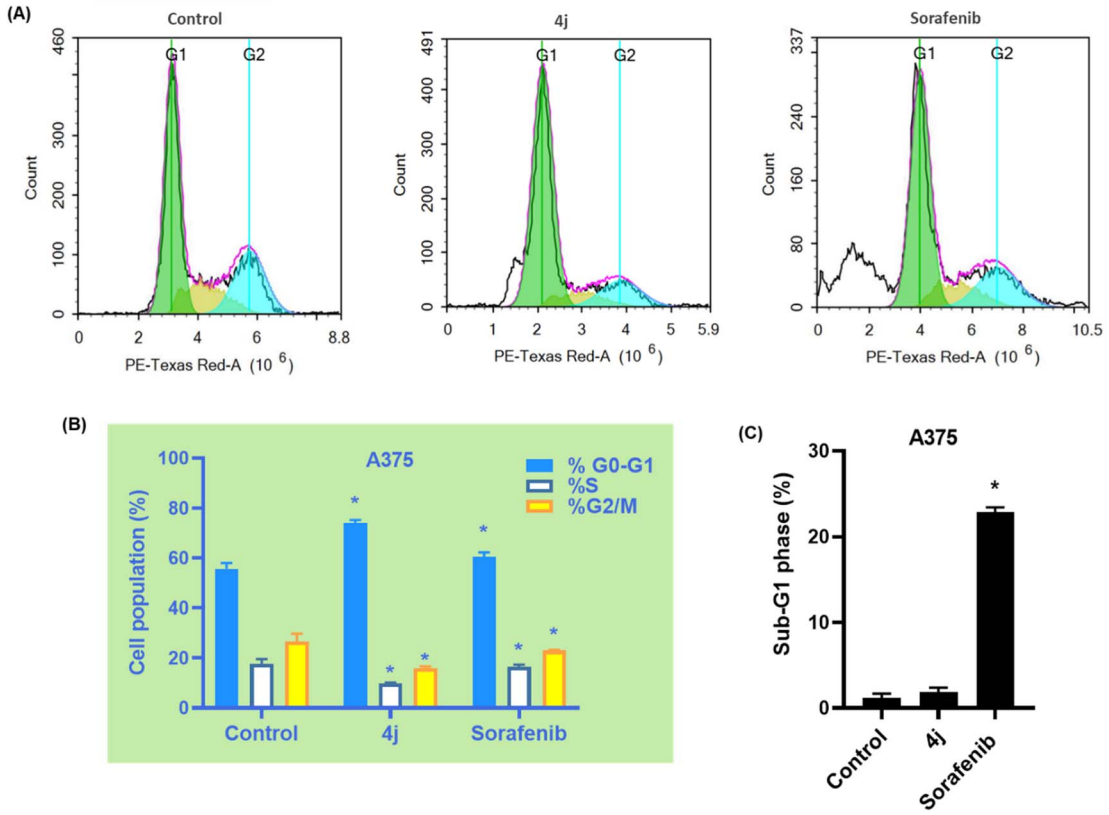


Fig. 3 (A) Cell cycle distribution in A375 cells after treatment with **4j** and sorafenib for 48 h determined using DNA cytometry analysis compared with a control (untreated cells). (B) Quantification of the percentage of cells in each phase of the cell cycle is depicted as a bar graph of mean ± SD; $n = 3$. (C) Sub-G1 phase was plotted alone as a proportion of total events. * Statistically significant difference from the control ($P < 0.05$).

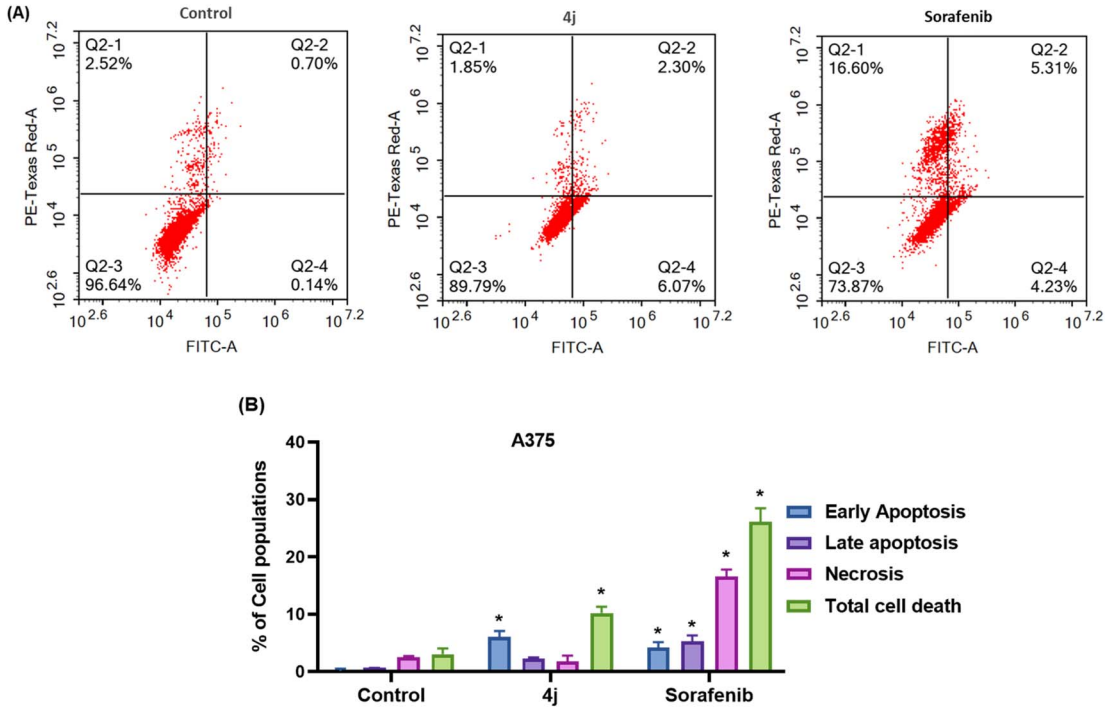


Fig. 4 (A) Evaluation of cell death modality (apoptosis/necrosis) after treatment with **4j** and sorafenib for 48 h in A375 cells, followed by double staining with Annexin-FITC/PI. (B) Different cell populations plotted as the percentage of total events. Data are presented as mean ± SD; $n = 3$. Total cell death calculated by combining apoptosis and necrosis. * Statistically significant difference from the control ($P < 0.05$).

the control untreated A375 cells with 0.14% early and 0.7% late apoptosis, respectively (Fig. 4A). These findings show that most of the cells underwent cell death by the apoptotic mode, suggesting that **4j** exerted its anticancer activity through the apoptosis route. This is consistent with the studies that reported apoptosis as a mechanism of cell death in cancer treatment by coumarin compounds.[48] However, treatment with **4j** did not induce notable necrotic cell death compared to the control cells (2.52% and 1.85%, respectively). This indicates that **4j** at its $IC_{50}$ concentration can induce apoptosis, mainly early apoptosis, of A375 melanoma cells but not necrosis. Furthermore, it arrested cells in the G1 phase, which promoted cell apoptosis in melanoma cells. Meanwhile, treatment with sorafenib showed a dramatic decrease in cell viability. Sorafenib treatment produced greater cell death than **4j** in A375, which was mainly necrotic (16.6%) ($p < 0.05$), and nearly the same percentage of apoptotic cell death (9.6%) compared with the **4j**-treated cells. This can be related to the sorafenib dose, which only modestly boosted apoptosis relative to necrosis.[53] It is also worth noting that the amount of necrosis did not correlate with apoptosis, indicating that distinct mechanisms are involved.[54]

**2.2.5. *In vitro* inhibition effect of 4j on the migration of melanoma cells.** One of the main reasons for the increased mortality of melanoma is its rapid progression and metastasis to lymph nodes and distant organs.[55] We used the scratch/wound healing assay to investigate the effects of **4j** and sorafenib on A375 melanoma cell migration (Fig. 5A and B), and we assessed the scratch closure daily until complete closure of the control untreated cells. At 0 h, the scratch line of all the groups revealed an insignificant change ($P > 0.5$) in the gap, indicating that the scratch technique was consistent.

Compound **4j** displayed a significant ($P < 0.05$) anti-metastasis effect by inhibiting A375 cell migration at all time intervals compared with the control untreated cells. Also, it showed a comparable effect to sorafenib anti-migratory activity. After 24 h, **4j** treatment postponed the migration tendency of A375 cancer cells, as evidenced by the 14.28% ± 2.13% delay in cell-free zone closure compared to 38.68% ± 0.89% for the untreated cells. After 48 h of **4j** treatment, a similar pattern was observed, with a delayed scratch closure of 17.57% ± 1.72% compared to 62.77% ± 1.78% in the control cells, demonstrating that **4j** may exert an anti-migratory effect in melanoma cancer cells. The following day (72 h), complete scratch closure was observed in the control group (100%); however, the scratch remained open in the **4j**-treated cells, with the scratch closure of 35.16% ± 2.45%, indicating that **4j** could exert a potent anti-migratory effect at this concentration (0.5 μM, nearly 1/2 $IC_{50}$ value). Similarly, compared to the untreated cells, the sorafenib-treated melanoma cells demonstrated delayed migration, which was slightly more potent than the **4j**-treated cells, with scratch closure of 9.15% ± 0.64%, 12.07% ± 1.8%, and 24.17% ± 1.32% at 24, 48, and 72 h, respectively.

## 2.3. Molecular modeling study

**2.3.1. Topological polar surface area (TPSA).** In this study we computed the topological polar surface area (TPSA) (Table 4) as a 2D descriptor that can help in the SAR study. TPSA can predict the drug-like properties of tested compounds and

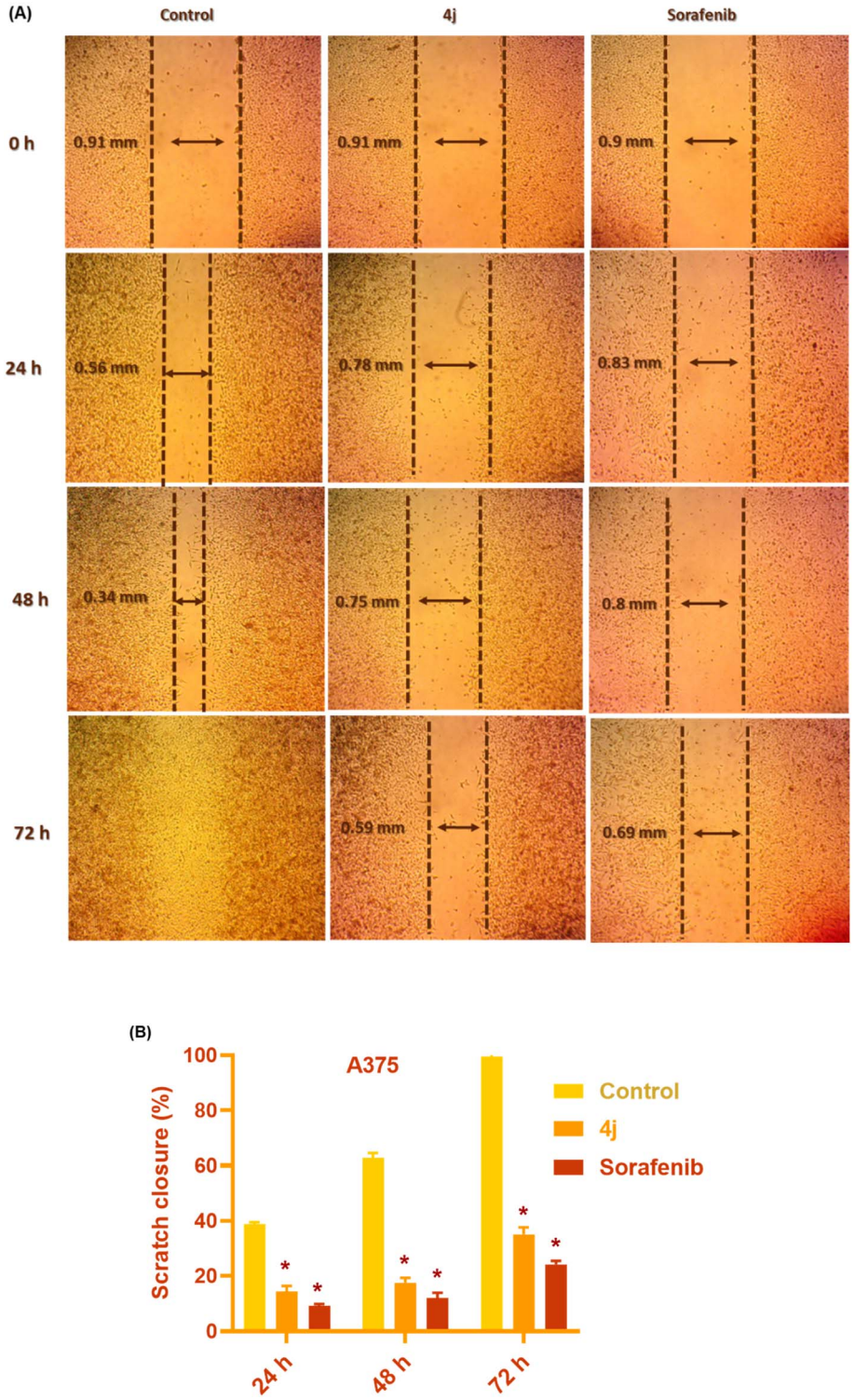


Fig. 5 Effect of **4j** and sorafenib on the migration of A375 cells. (A) Scratch widths were measured after **4j** and sorafenib treatment at 24, 48, and 72 h. (B) Data are plotted as scratch closure % at each time interval and presented as triplicates. * Statistically significant difference from the control ($P < 0.05$).

bioavailability properties such as transport and absorption. It was reported that any compound with a TPSA value of > 140 Å$^2$ will have poor absorption. Drug-like candidates will have a TPSA of <140 Å$^2$.[56–58] Accordingly the tested compounds were classified into three groups according to their TPSA values (Fig. 6 and Table 4).

(i) Compounds with TPSA = 102.6 Å$^2$, this group includes all compounds with trifluoromethoxy group at R2, halo atom (F, Cl, Br) at R3, and R1=H, *e.g.*, **4j**, **5j** and **6j**.

Table 4 Docking results against $BRAF^{V600E}$ (PBD = 2FB8) and TPSA

| Compound | $\Delta G$ (kcal mol$^{-1}$) | GBVI/WSA $\Delta G$ (kcal mol$^{-1}$) | RMSD (Å) | TPSA (Å$^2$) | Interacted residues |
|---|---|---|---|---|---|
| **4a** | −8.16 | −38.3 | 1.6 | 93.4 | Ile463, Asp594, Glu501 |
| **4b** | −6.45 | −30.75 | 2.75 | 84.6 | Trp531, Asp594 |
| **4c** | −8.77 | −38.91 | 2.59 | 84.6 | Asp594, Ile463 |
| **4d** | −8.57 | −42.5 | 1.2 | 93.4 | Cys532 |
| **4e** | −6.37 | −30.89 | 2.7 | 84.6 | Trp531 |
| **4f** | −9.04 | −41.35 | 1.44 | 84.6 | Phe593, Cys532 |
| **4g** | −8.82 | −39.05 | 1.41 | 93.4 | Cys532, Ala481, Lys483 |
| **4h** | −7.54 | −35.62 | 2.35 | 84.6 | Trp531, Cys532 |
| **4i** | −9.1 | −41.39 | 1.37 | 84.6 | Trp531, Phe583 |
| **4j** | −9.50 | −44.62 | 1.26 | 102.6 | Asp594, Thr529 |
| **5a** | −8.17 | −37.08 | 1.26 | 93.4 | Ile463, Glu501 |
| **5b** | −7.66 | −35.21 | 2.4 | 84.6 | Asn581, Asp594 |
| **5c** | −9.09 | −41.45 | 1.79 | 84.6 | Ile463 |
| **5d** | −8.52 | −38.46 | 1.04 | 93.4 | Cys532, Trp531, Asp594 |
| **5e** | −8.07 | −37.5 | 2.5 | 84.6 | Ile563, Ala481 |
| **5f** | −9.08 | −41.72 | 1.68 | 84.6 | Cys532, Trp531 |
| **5g** | −8.26 | −38.02 | 1.86 | 93.4 | Cys532, Ala481, Lys483 |
| **5h** | −8.83 | −38.55 | 1.41 | 84.6 | Trp531, Cys532 |
| **5i** | −9.11 | −41.98 | 0.82 | 84.6 | Phe593, Cys532 |
| **5j** | −8.92 | −41.36 | 2.72 | 102.6 | Cys532, Ile463, Lys481 |
| **6a** | −8.09 | −34.05 | 1.6 | 93.4 | Ile463, Asp594 |
| **6b** | −6.85 | −30.55 | 2.76 | 84.6 | Asn581 |
| **6c** | −8.59 | −38.87 | 1.28 | 84.6 | Ile463, Asp594 |
| **6d** | −8.20 | −38.42 | 1.52 | 93.4 | Cys532, Ala481, Lys483 |
| **6e** | −8.03 | −34.35 | 1.44 | 84.6 | Trp531, Cys532 |
| **6f** | −8.75 | −42.11 | 1.65 | 84.6 | Trp531, Phe583 |
| **6g** | −8.04 | −37.66 | 1.27 | 93.4 | Cys532, Ala481, Lys483 |
| **6h** | −7.46 | −34.79 | 2.5 | 84.6 | Trp531, Cys532 |
| **6i** | −8.72 | −39.11 | 1.27 | 84.6 | Trp531, Phe583 |
| **6j** | −8.65 | −38.87 | 1.22 | 102.6 | Ile463, Lys481 |
| **SB-590885** | −8.66 | −43.54 | 0.95 | 86.6 | Cys532, Ile463, Glu501 |
| **Sorafenib** | −8.26 | −42.93 | 0.97 | 92.36 | Cys532, Asp594, Glu501 |

(ii) Compounds with TPSA = 93.4 Å$^2$, this value is close to TPSA of sorafenib (92.36 Å$^2$), *e.g.*, compounds **4d**, **5d**, **4g**, **5g**, **4a**, **6d**, **5a**, **6g** and **6a**. All these compounds showed potent anticancer activity.

(iii) Compounds with TPSA = 84.6 Å$^2$, this value is close to that of the reference inhibitor SB-590885 (86.6 Å$^2$), *e.g.*, **5i**, **5f**, **4f**, **4i**, **5c**, **6f**, **4c**, **6c**, **5h**, **6i**, **5e** and **6e**. All these compounds also showed potent anticancer activity.

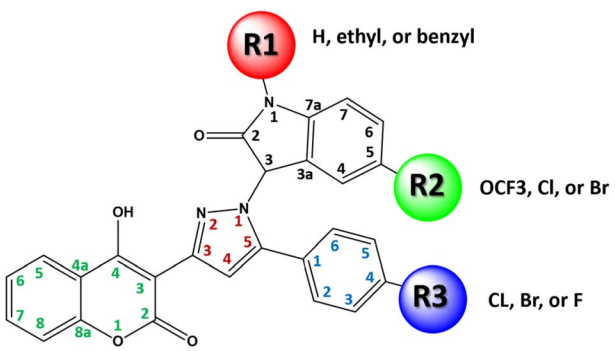


Fig. 6 Three main positions R1, R2, and R3 directly correlated with the anti-melanoma activity.

**2.3.2. Structure activity relationship.** According to the biological results, there are three main positions that are directly correlated with the activity of the tested compounds, *i.e.*, position N1 at the indolin-2-one scaffold, position 5 at the indolin-2-one scaffold, and position 4 at the phenyl ring, which are represented as R1, R2, and R3, respectively, in Fig. 6. All the compounds can be classified into three classes.

*2.3.2.1 Class I: compounds with no substitution at N1-indolin (R1 = H) and halo substitution at R2 and/or R3.* It was observed that the number of fluoro atom substitutions at R2 and R3 is very important for cytotoxic activity. The most active compound **4j** ($IC_{50}$ = 0.96 μM) with the highest number of F atoms (4 atoms) exhibited the highest TPSA value = 102.6 Å$^2$ among the compounds and the reference drugs given that the fluoro atom increases the lipophilicity and TPSA value. The replacement of F in compound **6** with Br or Cl yielded compound **6j** and **5j** with a decrease in cytotoxic activity ($IC_{50}$ = 4.37 and 4.17 μM, respectively). A further decrease in the number of F atoms resulted in a decrease in activity, for example, when the $OCF_3$ in compound **4j** was replaced with Br it yielded compound **4g** ($IC_{50}$ = 5.85 μM). This confirmed that the number of F atoms is directly proportional to the cytotoxic activity. The type of halo substitution at R2 and R3 can be ranked according to activity,

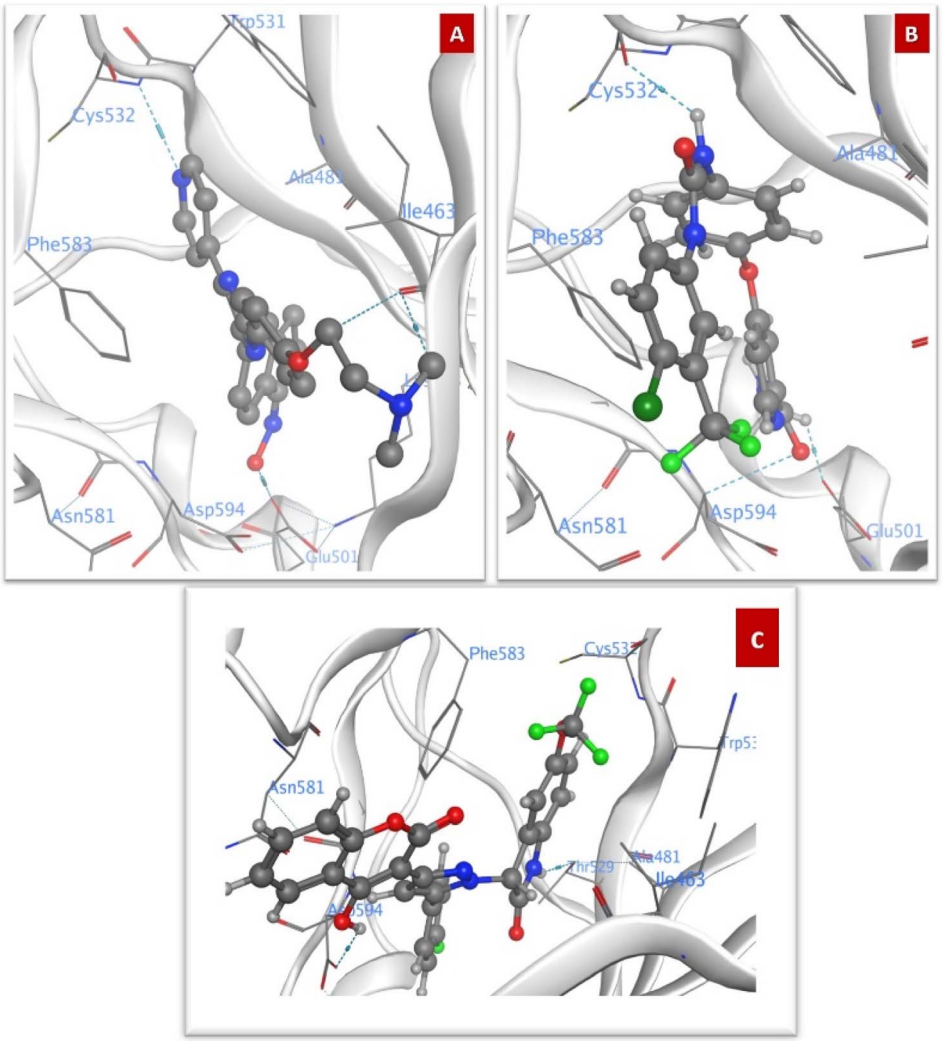


Fig. 7 Docking poses against $BRAF^{V600E}$ (A) **SB590885**, (B) **Sorafenib**, and (C) **4j**.

following the order of (Cl&F) > (Cl&Cl) > (Br&Br) and this can be observed in compound **4d** with Cl at R2 and F at R3 ($IC_{50}$ = 4.3 μM), which is more active than compound **5d** with Cl substitution at R2 and R3 ($IC_{50}$ = 5.43 μM), while compound **6g** with a Br atom at R2 and R3 was less active ($IC_{50}$ = 7.32 μM). In the case of compounds **4a**, **5a**, and **6a** having only one halo atom at R3 in the phenylpyrazolyl moiety, it was deduced that the presence of F substitution increased the activity, following the order of compound **4a** ($IC_{50}$ = 6.25 μM) > compound **5a** ($IC_{50}$ = 7.13 μM) > compound **6a** ($IC_{50}$ = 8.45 μM), which confirmed the importance of the presence of fluoro substitution, as discussed in the previous section. The compounds of this class (**4a**, **5a** and **6a**) exhibited the same TPSA value = 93.4 $Å^2$, which is close to that of sorafenib (92.36 $Å^2$).

*2.3.2.2 Class II: compounds with benzyl group at N1-indolin (R1 = benzyl) and halo substitution at R2 and/or R3.* The presence of a benzyl group in compounds **4c**, **5c** and **6c** was very important due to the hydrophobic interactions provided by the phenyl ring, which were oriented between hydrophobic residues Trp531, Phe583, and Ile463. Also, the methylene $–CH_2$ of the benzyl group was important for van der Waals formation to support the fitting of these compounds. The benzyl group increased the lipophilicity and decreased the TPSA value of these derivatives to reach 84.6 $Å^2$, which is close to that of SB-590885 = 86.6 $Å^2$ (Table 4) and may be correlated with their activity. The activity of **4c**, **5c** and **6c** was improved compared to the compounds in the previous class with $IC_{50}$ values of 3.8, 4.6, and 4.84 μM, respectively. Moreover, the presence of bromo substitution at R2 and R3 decreased the activity, as observed in compound **6i** ($IC_{50}$ = 5.47 μM), where the presence of fluoro substitution at the 4-position of the phenyl ring (R3) with either chloro or bromo substitution at the 5-position of the indolin-2-one scaffold (R2) improved the activity, as in compound **4f** ($IC_{50}$ = 1.1 μM) and compound **4i** ($IC_{50}$ = 1.28 μM). The substitution with two chloro atoms at both R2 and R3 retained the improved activity as in compound **5f** ($IC_{50}$ = 1.09 μM). The presence of chloro substitution at R2 and bromo substitution at R3 decreased the activity as in compound **6f** ($IC_{50}$ = 4.36 μM). The TPSA value of these compounds was 84.6 $Å^2$, which is close to that of SB-590885 = 86.6 $Å^2$ (Table 4).

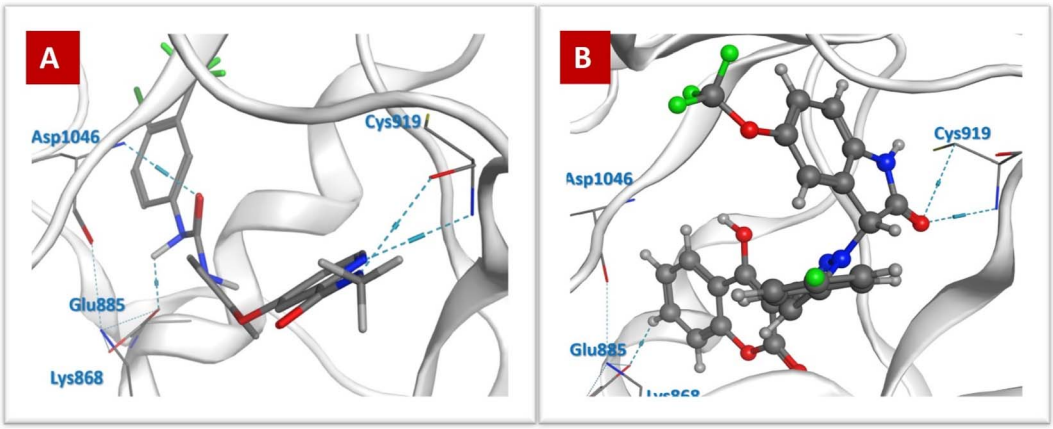


Fig. 8 Docking poses against VEGFR-2: (A) **Sorafenib** and (B) **4j**.

*2.3.2.3 Class III: compounds with ethyl at N1-indolin (R1 = ethyl).* This class showed some deviation from the previous observations, where the best activity was achieved by compound **5h** (R2═Br and R3═Cl) with an $IC_{50}$ value of 5.44 μM, which may need future investigation. In addition, dichloro substitution at R2 and R3 in compound **5e** showed good activity ($IC_{50}$ = 7.32 μM). However, the TPSA of these compounds was 84.6 Å$^2$, which is close to that of SB-590885.

**2.3.3. Molecular docking study against BRAF$^{V600E}$.** To determine the binding modes of the target compounds, molecular docking was performed within the BRAF$^{V600E}$ binding active site (**PBD** = **2FB8**). The docking results of the reference ligand SB590885 within the BRAF$^{V600E}$ binding active site showed three hydrogen bonds formed between Cys532 and C═N of the pyridine ring, between the dimethyl amino group in the side chain and Ile463 and between the hydroxyl group of oxime and Glu501 (Fig. 7A). Sorafenib also interacted by three hydrogen bonds, where one was formed between –NH of the urea group and Cys532, the other bond between the acetamide side chain and Asp594 and the last one with Glu501 (Fig. 7B). The molecular docking of **4j** with the highest Δ*G* value of −9.50 kcal mol$^{-1}$ against BRAF$^{V600E}$, revealed that the 4-hydroxy group formed a hydrogen bond with the –COOH group of Asp594 and the –NH of indoline formed a hydrogen bond with C═O of Thr529. The 5-(trifluoromethoxy) indolin-2-one scaffold was oriented and surrounded by hydrophobic residues, *i.e.*, Phe583, Ile463, and Trp531, with the possible formation of hydrophobic interactions (Fig. 7C and Table 4).

Compound **5j** showed the same orientation of the 5-(trifluoromethoxy) indolin-2-one scaffold surrounded by all the hydrophobic residues. It formed hydrogen bonds with Cys532, Ile463, and Lys481. Compound **6j** also formed the same interactions as **5j** with Ile463 and Lys481. Compound **4d** formed one hydrogen bond with Cys532, while compound **5d** formed three hydrogen bonds with Cys532, Trp531, and Asp594. Compound **6g** showed three hydrogen bonds with Cys532, Ala481 and Lys483. The coumarin ring in compound **4a** formed two hydrogen bonds with Asp594 and Glu501. The 4-bromophenyl ring in compound **5a** showed hydrophobic interactions with Ile463. The –NH of the pyrazole in compounds **4a**, **5a**, and **6a** interacted by a hydrogen bond with C═O of Ile463 and the C═O of coumarin in compound **6a** showed a hydrogen bond with Asp594 (Fig. S1A–I†).

The –$CH_2$ of benzyl moiety in compounds **4c** and **6c** formed van der Waals interactions with Ile463, while the same group in compound **4f** formed hydrophobic interactions with Phe583. The phenyl ring of the benzyl moiety of compound **6i** showed π–π interactions with Trp531 and Phe583. The –$CH_2$ of the benzyl moiety in compound **5f** formed hydrophobic interactions with Trp531 and Cys532 (Fig. S2A–F†). The docking of compounds with R1 = ethyl and R3 = halo substitution showed that compound **5b** formed two hydrogen bonds with Asn581 and Asp594. Compound **6b** showed a hydrogen bond with Asn581. The ethyl group in compound **4b** contributed to van der Waals interactions with Trp531 and the C═O of coumarin formed a hydrogen bond with Asp594. The pyrazole ring in compound **5e** contributed to van der Waals interactions with Ile463 and the C═O of coumarin formed a hydrogen bond with Ala481. The ethyl group in compound **6h** formed two van der Waals interactions with Trp531 and Cys532. Compound **4e** showed one van der Waals interaction between the ethyl group at R1 and Trp531 (Fig. S3A–F†).

**2.3.4. Molecular docking study against VEGFR-2.** The synthesized compounds were also docked in the VEGFR-2 binding pocket (**PBD** = **3VO3**). Sorafenib showed the best mode of binding, where it interacted with the important residues in the active site, *i.e.*, Asp1046, Cys919, and Glu886 (Fig. 8A). The top ranked compounds **4j**, **4i**, **4f**, **5f** and **5i** showed different binding interactions against VEGFR-2 and their binding mode was compared to that of sorafenib. Compound **4j** achieved the Δ*G* of −8.47 kcal mol$^{-1}$ and ranked second after sorafenib, which showed Δ*G* of −9.44 kcal mol$^{-1}$ (Table 5). Compound **4j** showed two hydrogen bonds with Cys919 and one hydrogen bond with Glu885 (Fig. 8B). The interaction with the Cys919 residue was a common feature among compounds **4j**, **4f**, **4i**, and **5i** and the reference drug. Compounds **4f** and **4i** formed hydrogen bonds with only Cys919. Compound **5f** showed

Table 5 Docking results against VEGFR-2 (PBD = 3VO3)

| Compound | $\Delta G$ (kcal mol$^{-1}$) | GBVI/WSA $\Delta G$ (kcal mol$^{-1}$) | RMSD (Å) | Interacted residues |
|---|---|---|---|---|
| **4a** | −7.65 | −36.99 | 1.35 | Glu885 |
| **4b** | −7.04 | −36.61 | 2.05 | Lys868 |
| **4c** | −8.23 | −36.6 | 1.83 | Cys919, Lys868 |
| **4d** | −7.42 | −39.21 | 1.57 | Cys919 |
| **4e** | −7.18 | −36.57 | 1.74 | Lys868 |
| **4f** | −8.21 | −33.3 | 1.95 | Cys919 |
| **4g** | −7.98 | −38.44 | 1.92 | Cys919 |
| **4h** | −7.17 | −35.63 | 1.82 | Lys868, Glu885 |
| **4i** | −7.86 | −40.31 | 1.81 | Cys919 |
| **4j** | −8.47 | −37.79 | 1.61 | Cys919, Glu885 |
| **5a** | −7.88 | −39.58 | 1.05 | Glu885 |
| **5b** | −7.17 | −37.35 | 2.33 | Lys868 |
| **5c** | −8.02 | −34.73 | 1.31 | Cys919, Lys868 |
| **5d** | −7.53 | −35.11 | 1.39 | Cys919 |
| **5e** | −7.71 | −34.67 | 2.12 | Lys868, Glu885 |
| **5f** | −7.62 | −37.01 | 1.70 | Asp1046 |
| **5g** | −7.27 | −36.17 | 1.42 | Cys919 |
| **5h** | −7.44 | −36.83 | 1.76 | Lys868, Glu885 |
| **5i** | −7.79 | −35.65 | 1.57 | Cys919, Lys868 |
| **5j** | −7.75 | −36.29 | 2.32 | Cys919, Glu885 |
| **6a** | −7.85 | −37.38 | 1.44 | Glu885 |
| **6b** | −7.15 | −32.09 | 1.54 | Lys868, Glu885 |
| **6c** | −7.10 | −35.68 | 1.11 | Cys919, Lys868 |
| **6d** | −7.54 | −38.08 | 2.77 | Cys919 |
| **6e** | −7.36 | −37.52 | 1.87 | Lys868, Glu885 |
| **6f** | −7.18 | −37.34 | 2.1 | Cys919, Lys868 |
| **6g** | −7.64 | −32.51 | 1.44 | Cys919 |
| **6h** | −7.60 | −37.66 | 1.29 | Lys868, Glu885 |
| **6i** | −7.95 | −35.55 | 1.72 | Cys919, Lys868 |
| **6j** | −7.70 | −35.81 | 1.93 | Cys919, Glu885 |
| **Sorafenib** | −9.44 | −46.54 | 1.47 | Asp1046, Cys919, Glu885 |

a hydrogen bond with Asp1046, while compound **5i** has two hydrogen bonds with Cys919 and Lys868 (Fig. S4A–F†).

The aforementioned information showed that the results of the *in silico* studies were consistent with that of the biological assays, where the most active compound **4j** with the $IC_{50}$ value of 0.96 μM against A375 cells and dual inhibition properties against $BRAF^{V600E}$/VEGFR-2 ($IC_{50}$ = 1.033 and 0.64 μM, respectively), revealed the highest $\Delta G$ value of −9.5 kcal mol$^{-1}$ against $BRAF^{V600E}$ and showed a significant $\Delta G$ of −8.47 kcal mol$^{-1}$ towards VEGFR-2. Moreover, compound **4j** displayed different types of interactions with essential catalytic sites in the active region of $BRAF^{V600E}$ and VEGFR-2.

**2.3.5. ADME prediction study.** The pharmacokinetic properties of compounds **4j**, **4f**, **4i**, **5f**, and **5i** were estimated, which showed the best anti-melanoma activity (Table S1†). The most promising compound **4j** showed high skin permeability with no skin sensitization, which can be used to interpret its activity and show its appropriate use against melanoma skin cancer. The human colon adenocarcinoma cell line (Caco-2) was used to predict the *in vivo* drug transport through the intestinal epithelium, where **4j** showed high predicted Caco-2 permeability and high intestinal absorption of 100%. Derivative **4j** showed high plasma protein binding with poor clearance and very low fraction of unbound drug. Furthermore, compound **4j** did not show any Ames toxicity or carcinogenicity.

## 3. Conclusion

In this study, a series of new coumarin derivatives bearing a pyrazolylindolin-2-one core was synthesized and evaluated for their anti-proliferative effects against human melanoma A375 cells as dual $BRAF^{V600E}$ and VEGFR-2 inhibitors. Most of the compounds displayed potent antiproliferative activity against A375 cells with $IC_{50}$ values in the range of 0.96–8.99 μM. Among them, compounds **4j**, **4f**, **4i**, **5f** and **5i** demonstrated potent cytotoxic activity ($IC_{50}$ = 0.96–1.28 μM) and good safety profile. Furthermore, compound **4j** exerted greater potent dual inhibitory activity against $BRAF^{V600E}$/VEGFR-2 than the reference drug sorafenib. The anticancer effect of **4j** was correlated with the inhibition of cell proliferation, boosting cell cycle arrest at the G0/G1 phase, induction of apoptosis, and inhibition of migration. Docking simulation was carried out for the active compounds to predict their binding modes in the $BRAF^{V600E}$ and VEGFR-2 protein active sites, revealing various interactions with the binding residues in the active site. The SAR study showed the correlation between the number of fluoro atoms and both TPSA and cytotoxic activity.

# 4. Experimental

## 4.1. Chemistry

Melting points were determined on an Electrothermal IA 9000 apparatus and were uncorrected. Elemental analyses were carried out at the Micro-analytical Central Services Laboratory, Faculty of Science, Cairo University, Egypt. $^1$H NMR and $^{13}$C NMR spectra were measured using a Bruker Avance II™ 400 MHz spectrometer (Bruker Biospin AG, Fällanden, Switzerland) in Prague, Czech Republic. $^{13}$C NMR spectra of compounds **4e**, **4h** and **5h** could not be acquired due to their precipitation from the solvent used (DMSO). The reactions were monitored by TLC (silica gel, aluminium sheets 60 F254, Merck) using chloroform/methanol (9.5 : 0.5 v/v) as the eluent and sprayed with iodine–potassium iodide solution. The key intermediates **3a–c** [47,48] and isatin derivatives **Ia–j** [59,60] and **4a** [47] were previously prepared.

**4.1.1. General procedure for the preparation of pyrazolyl indolin-2-one derivatives 4a–j, 5a–j and 6a–j.** A mixture of 1 mmol of pyrazoline compounds **3a** (0.32 g), **3b** (0.34 g) and/or **3c** (0.38 g) and isatin derivatives **Ia–j** (1 mmol) in absolute ethanol (20 mL) was refluxed for 8–10 h. After completion of the reaction, the obtained product was filtered, washed with ethanol, and recrystallized from acetic acid to obtain the desired target compounds **4a–j**, **5a–j** and **6a–j**, respectively.

*4.1.1.1 1-Ethyl-3-(5-(4-fluorophenyl)-3-(4-hydroxy-2-oxo-2H-chromen-3-yl)-1H-pyrazol-1-yl) indolin-2-one **4b**.* Yellow crystals, m.p. 277–278 °C, yield (0.35 g, 73%). $^1$H NMR (400 MHz, DMSO-$d_6$): $\delta$ = 1.15 (t, 3H, $J$ = 7.2 Hz, $CH_3$), 3.72 (q, 2H, $J$ = 6.4 Hz, $CH_2$), 6.32 (s, 1H, CH-indole), 7.06–7.09 (m, 1H, H–Ar), 7.18–7.28 (m, 4H, H–Ar), 7.34–7.44 (m, 5H, H–Ar), 7.64–7.70 (m, 2H, H–Ar), 7.84 (d, 1H, $J$ = 8.4 Hz, H–Ar), 13.06 (s, 1H, OH). $^{13}$C NMR (101 MHz, DMSO-$d_6$): $\delta$ = 12.79, 34.95, 60.71, 95.10, 106.89, 109.85, 115.49, 116.44, 116.66, 116.78, 123.21, 124.04, 124.87, 125.06, 125.24, 130.59, 132.06, 132.15, 143.20, 145.46, 147.77, 152.43, 159.70, 162.10, 163.41, 164.56, 171.26. Anal. calcd for $C_{28}H_{20}FN_3O_4$ (481.47): C, 69.85; H, 4.19; N, 8.73. Found: C, 70.00; H, 4.37; N, 8.89.

*4.1.1.2 1-Benzyl-3-(5-(4-fluorophenyl)-3-(4-hydroxy-2-oxo-2H-chromen-3-yl)-1H-pyrazol-1-yl) indolin-2-one **4c**.* Yellow crystals, m.p. 220–221 °C, yield (0.4 g, 74%). $^1$H NMR (400 MHz, DMSO-$d_6$): $\delta$ = 4.91 (d, 1H, $J$ = 15.6 Hz, $CH_a$-benzyl), 5.01 (d, 1H, $J$ = 16.0 Hz, $CH_b$-benzyl), 6.47 (s, 1H, CH-indole), 6.99 (d, 1H, $J$ = 8.0 Hz, H–Ar), (t, 1H, $J$ = 7.6 Hz, H–Ar), 7.26 (s, 1H, H–Ar). 7.30–7.46 (m, 11H, H–Ar). 7.67–7.71 (m, 1H, H–Ar), 7.79 (brs, 2H, H–Ar), 7.87 (d, 1H, $J$ = 6.8 Hz, H–Ar), 13.02 (s, 1H, OH). $^{13}$C NMR (101 MHz, DMSO-$d_6$): $\delta$ = 43.42, 60.42, 95.36, 106.83, 110.44, 115.52, 116.57, 116.79, 116.83, 123.48, 124.01, 124.99, 125.09, 125.13, 127.49, 127.99, 129.14, 130.48, 132.10, 132.19, 133.70, 136.15, 143.50, 145.86, 148.13, 152.55, 160.10, 162.17, 163.62, 164.62, 171.99. Anal. calcd for $C_{33}H_{22}FN_3O_4$ (543.15): C, 72.92; H, 4.08; N, 7.73. Found: C, 73.09; H, 4.22; N, 7.91.

*4.1.1.3 5-Chloro-3-(5-(4-fluorophenyl)-3-(4-hydroxy-2-oxo-2H-chromen-3-yl)-1H-pyrazol-1-yl) indolin-2-one **4d**.* Pale yellow powder, m.p. 294–295 °C, yield (0.38 g, 78%). $^1$H NMR (400 MHz, DMSO-$d_6$): $\delta$ = 6.24 (s, 1H, CH-indole), 6.96 (d, 1H, $J$ = 8.0 Hz, H–Ar), 7.22 (s, 1H, H–Ar), 7.36–7.44 (m, 6H, H–Ar), 7.66–7.70 (m, 1H, H–Ar), 7.76–7.79 (m, 2H, H–Ar), 7.88 (dd, 1H, $J$ = 1.6 and 8.0 Hz, H–Ar), 10.98 (s, 1H, NH), 13.13 (s, 1H, OH). $^{13}$C NMR (101 MHz, DMSO-$d_6$): $\delta$ = 60.70, 95.56, 106.73, 112.17, 115.50, 116.47, 116.69, 116.81, 124.11, 124.90, 125.11, 124.15, 125.55, 126.69, 127.72, 130.36, 132.16, 132.32, 133.69, 142.09, 145.84, 148.04, 152.53, 160.09, 163.61, 173.09 Anal. calcd for $C_{26}H_{15}ClFN_3O_4$ (487.86): C, 64.01; H, 3.10; N, 8.61. Found: C, 64.19; H, 3.24; N, 8.77.

*4.1.1.4 5-Chloro-1-ethyl-3-(5-(4-fluorophenyl)-3-(4-hydroxy-2-oxo-2H-chromen-3-yl)-1H-pyrazol-1-yl)indolin-2-one **4e**.* Yellow powder, m.p. 297–298 °C, yield (0.37 g, 72%). $^1$H NMR (400 MHz, DMSO-$d_6$): $\delta$ = 1.13 (t, 3H, $J$ = 7.2 Hz, $CH_3$), 3.71 (q, 2H, $J$ = 7.2 Hz, $CH_2$), 6.32 (s, 1H, CH-indole), 7.22–7.26 (m, 2H, H–Ar), 7.36–7.45 (m, 4H, H–Ar), 7.48–7.51 (m, 2H, H–Ar), 7.67–7.75 (m, 3H, H–Ar), 7.88 (dd, 1H, $J$ = 1.2 and 7.6 Hz, H–Ar), 13.03 (s, 1H, OH). Anal. calcd for $C_{28}H_{19}ClFN_3O_4$ (515.91): C, 65.18; H, 3.71; N, 8.14. Found: C, 65.36; H, 3.90; N, 8.32.

*4.1.1.5 1-Benzyl-5-chloro-3-(5-(4-fluorophenyl)-3-(4-hydroxy-2-oxo-2H-chromen-3-yl)-1H-pyrazol-1-yl) indolin-2-one **4f**.* Violet crystals, m.p. 223–225 °C, yield (0.45 g, 78%). $^1$H NMR (400 MHz, DMSO-$d_6$): $\delta$ = 4.90 (d, 1H, $J$ = 16.0 Hz, CH-benzyl), 5.02 (d, 1H, $J$ = 16.0 Hz, CH-benzyl), 6.47 (s, 1H, CH-indole), 7.01 (d, 1H, $J$ = 8.8 Hz, H–Ar), 7.26 (s, 1H, H–Ar). 7.29–7.45 (m, 10H, H–Ar). 7.53 (brs, IH, H–Ar) 7.66–7.70 (m, 1H, H–Ar), 7.80–7.83 (m, 2H, H–Ar), 7.87 (dd, 1H, $J$ = 1.6 and 8.0 Hz, H–Ar), 12.97 (s, 1H, OH). $^{13}$C NMR (101 MHz, DMSO-$d_6$): $\delta$ = 43.49, 60.17, 95.36, 106.89, 111.87, 115.47, 116.53, 116.74, 116.81, 124.03, 124.98, 125.07, 125.10, 125.49, 127.06, 127.45, 127.65, 128.06, 129.17, 130.33, 132.22, 132.30, 133.71, 135.81, 142.49, 146.10, 148.35, 152.54, 160.09, 162.21, 163.64, 164.66, 171.75. Anal. calcd for $C_{33}H_{21}ClFN_3O_4$ (577.12): C, 68.57; H, 3.66; N, 7.27. Found: C, 68.75; H, 3.83; N, 7.44.

*4.1.1.6 5-Bromo-3-(5-(4-fluorophenyl)-3-(4-hydroxy-2-oxo-2H-chromen-3-yl)-1H-pyrazol-1-yl) indolin-2-one **4g**.* White powder, m.p. 295–296 °C, yield (0.36 g, 68%). $^1$H NMR (400 MHz, DMSO-$d_6$): $\delta$ = 6.23 (s, 1H, CH-indole), 6.91 (d, 1H, $J$ = 8.4 Hz, H–Ar), 7.21 (s, 1H, H–Ar), 7.35–7.43 (m, 4H, H–Ar), 7.52 (s, 2H, H–Ar), 7.65–7.69 (m, 1H, H–Ar), 7.77(brt, 2H, H–Ar), 7.87 (d, 1H, $J$ = 7.6 Hz, H–Ar), 10.98 (s, 1H, NH), 13.14 (s, 1H, OH). $^{13}$C NMR (101 MHz, DMSO-$d_6$): $\delta$ = 60.61, 95.41, 106.72, 112.67, 114.30, 115.50, 116.46, 116.68, 116.81, 124.12, 124.90, 125.15, 128.09, 128.22, 132.16, 132.25, 133.21, 133.69, 142.51, 145.85, 148.05, 152.53, 162.16, 163.62, 172.97. Anal. calcd for $C_{26}H_{15}BrFN_3O_4$ (532.31): C, 58.66; H, 2.84; N, 7.89. Found: C, 58.85; H, 3.01; N, 8.09.

*4.1.1.7 5-Bromo-1-ethyl-3-(5-(4-fluorophenyl)-3-(4-hydroxy-2-oxo-2H-chromen-3-yl)-1H-pyrazol-1-yl) indolin-2-one **4h**.* Yellow crystals, m.p. 287–289 °C, yield (0.4 g, 71%). $^1$H NMR (400 MHz, DMSO-$d_6$): $\delta$ = 1.03 (t, 3H, $J$ = 6.0 Hz, $CH_3$), 3.66 (q, 2H, $J$ = 7.2 Hz, $CH_2$), 6.29 (s, 1H, CH-indole), 7.09 (s, 1H, H–Ar), 7.16–7.25 (m, 4H, H–Ar), 7.39–7.46 (m, 2H, H–Ar), 7.69 (d, 1H, $J$ = 2.0 Hz, $CH_2$), 7.80–7.84 (m, 2H, H–Ar), 7.94–7.98 (m, 2H, H–Ar), 13.31 (s, 1H, OH). Anal. calcd for $C_{28}H_{19}BrFN_3O_4$ (559.05): C, 60.01; H, 3.42; N, 7.50. Found: C, 60.12; H, 3.51; N, 7.67.

*4.1.1.8 1-Benzyl-5-bromo-3-(5-(4-fluorophenyl)-3-(4-hydroxy-2-oxo-2H-chromen-3-yl)-1H-pyrazol-1-yl)indolin-2-one **4i**.* Yellow

powder, m.p. 247–249 °C, yield (0.41 g, 66%). $^1$H NMR (400 MHz, DMSO-$d_6$): $\delta$ = 4.90 (d, 1H, $J$ = 16.0 Hz, $CH_a$-benzyl), 5.02 (d, 1H, $J$ = 16.00 Hz, $CH_b$-benzyl), 6.47 (s, 1H, CH-indole), 6.96 (d, 1H, $J$ = 8.4 Hz, H–Ar), 7.26 (s, 1H, H–Ar), 7.29–7.45 (m, 9H, H–Ar), 7.54 (dd, 1H, $J$ = 1.6 and 8.4 Hz, H–Ar), 7.63 (brs, 1H, H–Ar), 7.68–7.72 (m, 1H, H–Ar), 7.80–7.83 (m, 2H, H–Ar), 7.88 (dd, 1H, $J$ = 1.8 and 8.0 Hz, H–Ar), 13.00 (s, 1H, OH). $^{13}$C NMR (101 MHz, DMSO-$d_6$): $\delta$ = 43.45, 60.09, 95.37, 106.87, 112.37, 115.31, 115.49, 116.53, 116.75, 116.84, 124.06, 125.01, 125.10, 127.39, 127.43, 128.07, 128.15, 129.18, 132.23, 132.32, 133.20, 133.75, 135.80, 142.92, 148.34, 152.56, 160.10, 162.21, 163.66, 164.66, 171.65. Anal. calcd for $C_{33}H_{21}BrFN_3O_4$ (621.06): C, 63.68; H, 3.40; N, 6.75. Found: C, 63.85; H, 3.58; N, 6.86.

*4.1.1.9 3-(5-(4-Fluorophenyl)-3-(4-hydroxy-2-oxo-2H-chromen-3-yl)-1H-pyrazol-1-yl)-5 (trifluoromethoxy) indolin-2-one* ***4j****.* Yellow crystals, m.p. 293–294 °C, yield (0.4 g, 74%). $^1$H NMR (400 MHz, DMSO-$d_6$): $\delta$ = 6.32 (s, 1H, CH-indole), 7.02 (d, 1H, $J$ = 8.4 Hz, H–Ar), 7.22 (s, 1H, H–Ar), 7.35–7.44 (m, 6H, H–Ar), 7.66–7.70 (m, 1H, H–Ar), 7.76 (brs, 2H, H–Ar), 7.87 (dd, 1H, $J$ = 0.8 and 7.6 Hz, H–Ar), 11.02 (s, 1H, NH), 13.11 (s, 1H, OH). $^{13}$C NMR (101 MHz, DMSO-$d_6$): $\delta$ = 60.96, 95.40, 106.88, 111.62, 115.49, 116.39, 116.61, 116.82, 119.56, 121.85, 123.78, 124.07, 124.92, 125.17, 127.30, 132.13, 132.22, 133.70, 142.38, 143.85, 147.94, 152.53, 160.09, 162.14, 163.60, 173.50. Anal. calcd for $C_{27}H_{15}F_4N_3O_5$ (537.41): C, 60.34; H, 2.81; N, 7.82. Found: C, 60.51; H, 2.87; N, 7.99.

*4.1.1.10 3-(5-(4-Chlorophenyl)-3-(4-hydroxy-2-oxo-2H-chromen-3-yl)-1H-pyrazol-1-yl)indolin-2-one* ***5a****.* Rose crystals, m.p. 285–287 °C, yield (0.34 g, 72%). $^1$H NMR (400 MHz, DMSO-$d_6$): $\delta$ = 6.21 (s, 1H, CH-indole), 6.92 (d, 1H, $J$ = 7.6 Hz, H–Ar), 6.95(td, 1H, $J$ = 0.8 and 6.8 Hz, H–Ar), 7.17 (d, 1H, $J$ = 7.6 Hz, H–Ar), 7.20 (s, 1H, H–Ar), 7.28–7.39 (m, 3H, H–Ar), 7.58–7.65 (m, 3H, H–Ar), 7.70 (d, 2H, $J$ = 8.0 Hz, H–Ar), 7.81 (dd, 1H, $J$ = 1.6 and 8.0 Hz, H–Ar), 10.84 (s, 1H, NH), 13.11 (s, 1H, OH). $^{13}$C NMR (101 MHz, DMSO-$d_6$): $\delta$ = 60.76, 94.81, 106.75, 110.36, 115.02, 116.30, 122.56, 123.90, 124.73, 125.08, 125.56, 127.41, 129.47, 130.35, 131.33, 133.50, 134.94, 142.90, 145.28, 147.75, 152.27, 159.92, 163.41, 173.07. Anal. calcd for $C_{26}H_{16}ClN_3O_4$ (469.87): C, 66.46; H, 3.43; N, 8.94. Found: C, 66.62; H, 3.55; N, 9.08.

*4.1.1.11 3-(5-(4-Chlorophenyl)-3-(4-hydroxy-2-oxo-2H-chromen-3-yl)-1H-pyrazol-1-yl)-1-ethylindolin-2-one* ***5b****.* Off white powder, m.p. 245–246 °C, yield (0.37 g, 74%). $^1$H NMR (400 MHz, DMSO-$d_6$): $\delta$ = 1.15 (t, 3H, $J$ = 7.2 Hz, $CH_3$), 3.72 (q, 2H, $J$ = 8.0 Hz, $CH_2$), 6.34 (s, 1H, CH-indole), 7.06–7.09 (m, 1H, H–Ar), 7.19–7.29 (m, 5H, H–Ar), 7.35–7.45 (m, 4H, H–Ar), 7.60–7.71 (m, 2H, H–Ar), 7.85 (d, 1H, $J$ = 7.2 Hz, H–Ar), 13.08 (s, 1H, OH). $^{13}$C NMR (101 MHz, DMSO-$d_6$): $\delta$ = 12.61, 35.15, 60.68, 95.49, 107.06, 110.07, 115.31, 116.18, 123.12, 124.07, 124.90, 125.10, 125.21, 127.51, 129.52, 131.54, 133.68, 135.12, 137.08, 143.40, 147.94, 152.51, 160.08, 163.60, 171.23. Anal. calcd for $C_{28}H_{20}ClN_3O_4$ (497.92): C, 67.54; H, 4.05; N, 8.44. Found: C, 67.72; H, 4.19; N, 8.55.

*4.1.1.12 1-Benzyl-3-(5-(4-chlorophenyl)-3-(4-hydroxy-2-oxo-2H-chromen-3-yl)-1H-pyrazol-1-yl)indolin-2-one* ***5c****.* Yellow crystals, m.p. 235–237 °C, yield (0.41 g, 73%). $^1$H NMR (400 MHz, DMSO-$d_6$): $\delta$ = 4.87 (d, 1H, $J$ = 16.0 Hz, $CH_a$-benzyl), 4.99 (d, 1H, $J$ = 15.6 Hz, $CH_b$-benzyl), 6.45 (s, 1H, CH-indole), 6.96 (d, 1H, $J$ = 8.0 Hz, H–Ar), 7.00 (t, 1H, $J$ = 7.6 Hz, H–Ar), 7.25 (s, 1H, H–Ar). 7.26–7.40 (m, 9H, H–Ar). 7.60–7.66 (m, 3H, H–Ar), 7.73–7.75 (m, 2H, H–Ar), 7.82 (dd, 1H, $J$ = 1.6 and 8.0 Hz, H–Ar), 13.00 (s, 1H, OH). $^{13}$C NMR (101 MHz, DMSO-$d_6$): $\delta$ = 43.43, 60.45, 95.34, 106.89, 110.45, 115.48, 116.82, 123.50, 124.01, 124.99, 125.07, 125.12, 127.48, 127.52, 127.99, 129.14, 129.70, 130.50, 131.55, 133.71, 135.19, 136.12, 143.49, 145.72, 148.22, 152.54, 160.09, 163.61, 171.96. Anal. calcd for $C_{33}H_{22}ClN_3O_4$ (559.12): C, 70.78; H, 3.96; N, 7.50. Found: C, 70.91; H, 4.12; N, 7.66.

*4.1.1.13 5-Chloro-3-(5-(4-chlorophenyl)-3-(4-hydroxy-2-oxo-2H-chromen-3-yl)-1H-pyrazol-1-yl) indolin-2-one* ***5d****.* Pale yellow powder, m.p. > 300 °C, yield (0.34 g, 67%). $^1$H NMR (400 MHz, DMSO-$d_6$): $\delta$ = 6.26 (s, 1H, CH-indole), 6.97 (d, 1H, $J$ = 8.0 Hz, H–Ar), 7.24 (s, 1H, H–Ar), 7.36–7.46 (m, 4H, H–Ar), 7.63–7.71 (m, 3H, H–Ar), 7.74 (d, 2H, $J$ = 8.4 Hz, H–Ar), 7.88–7.90 (m, 1H, H–Ar), 10.99 (s, 1H, NH), 13.11 (s, 1H, OH). $^{13}$C NMR (101 MHz, DMSO-$d_6$): $\delta$ = 60.75, 95.40, 106.79, 112.19, 115.49, 116.82, 124.13, 124.92, 125.59, 126.70, 127.53, 127.68, 129.60, 130.38, 131.62, 133.72, 135.14, 142.10, 145.69, 148.13, 152.54, 160.09, 163.63, 173.06. Anal. calcd for $C_{26}H_{15}Cl_2N_3O_4$ (504.32): C, 61.92; H, 3.00; N, 8.33. Found: C, 62.09; H, 3.16; N, 8.45.

*4.1.1.14 5-Chloro-3-(5-(4-chlorophenyl)-3-(4-hydroxy-2-oxo-2H-chromen-3-yl)-1H-pyrazol-1-yl)-1-ethylindolin-2-one* ***5e****.* Off white powder, m.p. 259–260 °C, yield (0.37 g, 69%). $^1$H NMR (400 MHz, DMSO-$d_6$): $\delta$ = 1.13 (t, 3H, $J$ = 6.8 Hz, $CH_3$), 3.72 (q, 2H, $J$ = 7.2 Hz, $CH_2$), 6.34 (s, 1H, CH-indole), 7.25 (s, 1H, H–Ar). 7.36–7.40 (m, 1H, H–Ar), 7.42 (d, 1H, $J$ = 8.0 Hz, H–Ar), 7.49–7.52 (m, 2H, H–Ar), 7.62–7.77 (m, 6H, H–Ar), 7.87 (dd, 1H, $J$ = 1.6 and 8.0 Hz, H–Ar), 13.00 (s, 1H, OH). $^{13}$C NMR (101 MHz, DMSO-$d_6$): $\delta$ = 12.68, 35.20, 60.33, 95.39, 106.99, 111.36, 115.48, 116.82, 124.14, 124.91, 125.49, 127.15, 127.32, 127.48, 129.58, 130.41, 131.66, 133.73, 135.16, 142.45, 145.59, 148.17, 152.54, 160.10, 163.64, 171.00. Anal. calcd for $C_{28}H_{19}Cl_2N_3O_4$ (531.07): C, 63.17; H, 3.60; N, 7.89. Found: C, 63.26; H, 3.77; N, 8.05.

*4.1.1.15 1-Benzyl-5-chloro-3-(5-(4-chlorophenyl)-3-(4-hydroxy-2-oxo-2H-chromen-3-yl)-1H-pyrazol-1-yl)indolin-2-one* ***5f****.* Violet crystals, m.p. 207–209 °C, yield (0.39 g, 66%). $^1$H NMR (400 MHz, DMSO-$d_6$): $\delta$ = 4.91 (d, 1H, $J$ = 15.6 Hz, CH-benzyl), 5.03 (d, 1H, $J$ = 15.6 Hz, CH-benzyl), 6.49 (s, 1H, CH-indole), 7.02 (d, 1H, $J$ = 8.8 Hz, H–Ar), 7.28 (s, 1H, H–Ar). 7.30–7.44 (m, 8H, H–Ar). 7.53(brs, 1H, H–Ar) 7.65–7.80 (m, 5H, H–Ar), 7.87 (dd, 1H, $J$ = 1.6 and 8.0 Hz, H–Ar), 13.10 (s, 1H, OH). $^{13}$C NMR (101 MHz, DMSO-$d_6$): $\delta$ = 43.49, 60.21, 95.34, 106.95, 111.90, 115.49, 116.83, 124.06, 124.99, 125.54, 127.02, 127.38, 127.44, 127.65, 128.07, 129.13, 129.18, 129.66, 130.35, 131.68, 133.75, 135.22, 135.82, 142.50, 145.97, 148.44, 152.57, 160.09, 163.68, 171.72. Anal. calcd for $C_{33}H_{21}Cl_2N_3O_4$ (593.09): C, 66.68; H, 3.56; N, 7.07. Found: C, 66.79; H, 3.69; N, 7.22.

*4.1.1.16 5-Bromo-3-(5-(4-chlorophenyl)-3-(4-hydroxy-2-oxo-2H-chromen-3-yl)-1H-pyrazol-1-yl)indolin-2-one* ***5g****.* Buff powder, m.p. 296–297 °C, yield (0.35 g, 64%). $^1$H NMR (400 MHz, DMSO-$d_6$): $\delta$ = 6.26 (s, 1H, CH-indole), 6.92 (d, 1H, $J$ = 8.8 Hz, H–Ar), 7.24 (s, 1H, H–Ar), 7.35 (t, 1H, $J$ = 7.6 Hz, H–Ar), 7.41 (d, 1H, $J$ = 8.4 Hz, H–Ar), 7.53 (s, 2H, H–Ar), 7.63–7.69 (m, 3H, H–Ar), 7.74 (d, 2H, $J$ = 7.6 Hz, H–Ar), 7.87 (d, 1H, $J$ = 7.6 Hz, H–Ar), 10.99 (s, 1H, NH), 13.09 (s, 1H, OH). $^{13}$C NMR (101 MHz, DMSO-$d_6$): $\delta$ = 60.65, 95.39, 106.79, 112.68, 114.32, 115.48, 116.80, 124.12,

124.89, 127.53, 128.04, 128.26, 129.04, 129.59, 131.62, 133.22, 133.70, 135.14, 142.51, 145.69, 148.13, 152.53, 160.07, 163.61, 172.93. Anal. calcd for $C_{26}H_{15}BrClN_3O_4$ (548.77): C, 56.90; H, 2.76; N, 7.66. Found: C, 57.10; H, 2.92; N, 7.77.

*4.1.1.17 5-Bromo-3-(5-(4-chlorophenyl)-3-(4-hydroxy-2-oxo-2H-chromen-3-yl)-1H-pyrazol-1-yl)-1-ethylindolin-2-one* ***5h***. Brown powder, m.p. > 300 °C, yield (0.45 g, 78%). $^1$H NMR (400 MHz, DMSO-$d_6$): $\delta$ = 1.12 (t, 3H, $J$ = 6.8 Hz, $CH_3$), 3.68 (q, 2H, $J$ = 6.8 Hz, $CH_2$), 6.31 (s, 1H, CH-indole), 7.16–7.87 (m, 12H, H–Ar), 12.99 (s, 1H, OH). Anal. calcd for $C_{28}H_{19}BrClN_3O_4$ (575.02): C, 58.30; H, 3.32; N, 7.28. Found: C, 58.48; H, 3.51; N, 7.45.

*4.1.1.18 1-Benzyl-5-bromo-3-(5-(4-chlorophenyl)-3-(4-hydroxy-2-oxo-2H-chromen-3-yl)-1H-pyrazol-1-yl)indolin-2-one* ***5i***. Buff powder, m.p. 228–229 °C, yield (0.52 g, 82%). $^1$H NMR (400 MHz, DMSO-$d_6$): $\delta$ = 4.90 (d, 1H, $J$ = 15.6 Hz, $CH_a$-benzyl), 5.02 (d, 1H, $J$ = 15.6 Hz, $CH_b$-benzyl), 6.49 (s, 1H, CH-indole), 6.97 (d, 1H, $J$ = 8.8 Hz, H–Ar), 7.29 (s, 1H, H–Ar), 7.34–7.45 (m, 7H, H–Ar), 7.55 (d, 1H, $J$ = 8.4 Hz, H–Ar), 7.64 (brs, 1H, H–Ar), 7.67–7.73 (m, 3H, H–Ar), 7.79–7.81 (m, 2H, H–Ar), 7.88 (d, 1H, $J$ = 6.8 Hz, H–Ar), 12.93 (s, 1H, OH). $^{13}$C NMR (101 MHz, DMSO-$d_6$): $\delta$ = 43.46, 60.11, 95.35, 106.88, 112.39, 115.32, 115.47, 116.83, 123.97, 124.06, 125.00, 125.08, 127.34, 127.43, 127.85, 128.06, 128.20, 129.18, 131.77, 131.91, 132.58, 133.21, 133.76, 135.80, 142.93, 146.06, 148.46, 152.56, 160.08, 163.65, 171.61. Anal. calcd for $C_{33}H_{21}BrClN_3O_4$ (637.04): C, 62.04; H, 3.31; N, 6.58. Found: C, 62.19; H, 3.49; N, 6.77.

*4.1.1.19 3-(5-(4-Chlorophenyl)-3-(4-hydroxy-2-oxo-2H-chromen-3-yl)-1H-pyrazol-1-yl)-5-(trifluoromethoxy)indolin-2-one* ***5j***. Yellow powder, m.p. 299–300 °C, yield (0.34 g, 61%). $^1$H NMR (400 MHz, DMSO-$d_6$): $\delta$ = 6.34 (s, 1H, CH-indole), 7.03 (d, 1H, $J$ = 8.4 Hz, H–Ar), 7.24 (s, 1H, H–Ar), 7.36–7.44 (m, 4H, H–Ar), 7.61–7.70 (m, 3H, H–Ar), 7.74–7.83 (m, 2H, H–Ar), 7.86 (dd, 1H, $J$ = 1.2 and 8.0 Hz, H–Ar), 11.04 (s, 1H, NH), 13.00 (s, 1H, OH). $^{13}$C NMR (101 MHz, DMSO-$d_6$): $\delta$ = 60.98, 95.38, 106.94, 111.65, 115.47, 116.82, 119.32, 119.60, 121.85, 123.80, 124.08, 124.92, 127.25, 127.56, 129.53, 131.59, 133.71, 135.11, 142.39, 143.86, 145.61, 148.02, 152.53, 160.09, 163.60, 173.46. Anal. calcd for $C_{27}H_{15}ClF_3N_3O_5$(553.87): C, 58.55; H, 2.73; N, 7.59. Found: C, 58.68; H, 2.91; N, 7.78.

*4.1.1.20 3-(5-(4-Bromophenyl)-3-(4-hydroxy-2-oxo-2H-chromen-3-yl)-1H-pyrazol-1-yl)indolin-2-one* ***6a***. Rose powder, m.p. 291–292 °C, yield (0.42 g, 81%). $^1$H NMR (400 MHz, DMSO-$d_6$): $\delta$ = 6.25 (s, 1H, CH-indole), 6.96 (d, 1H, $J$ = 8.0 Hz, H–Ar), 6.99 (td, 1H, $J$ = 0.4 and 3.6 Hz, H–Ar), 7.21 (d, 1H, $J$ = 7.6 Hz, H–Ar), 7.24 (s, 1H, H–Ar), 7.32–7.39 (m, 2H, H–Ar), 7.41 (d, 1H, $J$ = 8.0 Hz, H–Ar), 7.65–7.69 (m, 3H, H–Ar), 7.76 (d, 2H, $J$ = 8.4 Hz, H–Ar), 7.86 (dd, 1H, $J$ = 1.6 and 8.0 Hz, H–Ar), 10.87 (s, 1H, NH), 13.11 (s, 1H, OH). $^{13}$C NMR (101 MHz, DMSO-$d_6$): $\delta$ = 60.92, 95.37, 106.69, 110.73, 115.49, 116.81, 122.72, 123.85, 124.07, 124.90, 125.21, 125.73, 127.93, 130.51, 131.71, 132.56, 133.67, 143.03, 145.52, 147.93, 152.52, 160.03, 163.57, 173.29. Anal. calcd for $C_{26}H_{16}BrN_3O_4$ (514.32): C, 60.72; H, 3.14; N, 8.17. Found: C, 60.92; H, 3.33; N, 8.32.

*4.1.1.21 3-(5-(4-Bromophenyl)-3-(4-hydroxy-2-oxo-2H-chromen-3-yl)-1H-pyrazol-1-yl)-1-ethylindolin-2-one* ***6b***. Yellow powder, m.p. 273–275 °C, yield (0.41 g, 76%). $^1$H NMR (400 MHz, DMSO-$d_6$): $\delta$ = 1.11 (t, 3H, $J$ = 6.8 Hz, $CH_3$), 3.68 (q, 2H, $J$ = 7.2 Hz, $CH_2$), 6.30 (s, 1H, CH-indole), 7.02–7.06 (m, 1H, H–Ar), 7.15–7.24 (m, 3H, H–Ar), 7.30–7.41 (m, 3H, H–Ar), 7.58–7.64 (m, 3H, H–Ar), 7.69 (d, 2H, $J$ = 8.0 Hz, H–Ar), 7.80 (dd, 1H, $J$ = 1.2 and 8.0 Hz, H–Ar), 12.97 (s, 1H, OH). $^{13}$C NMR (101 MHz, DMSO-$d_6$): $\delta$ = 12.74, 35.00, 60.54, 95.33, 106.86, 109.83, 115.42, 116.75, 123.20, 123.82, 124.02, 124.85, 125.06, 125.17, 127.82, 129.61, 130.58, 131.70, 132.47, 133.63, 143.36, 145.34, 147.93, 152.46, 160.04, 163.51, 171.17. Anal. calcd for $C_{28}H_{20}BrN_3O_4$ (542.38): C, 62.00; H, 3.72; N, 7.75. Found: C, 62.12; H, 3.90; N, 7.89.

*4.1.1.22 1-Benzyl-3-(5-(4-bromophenyl)-3-(4-hydroxy-2-oxo-2H-chromen-3-yl)-1H-pyrazol-1-yl)indolin-2-one* ***6c***. Off white powder, m.p. 239–241 °C, yield (0.47 g, 78%). $^1$H NMR (400 MHz, DMSO-$d_6$): $\delta$ = 4.91 (d, 1H, $J$ = 16.0 Hz, $CH_a$-benzyl), 5.02 (d, 1H, $J$ = 16.0 Hz, $CH_b$-benzyl), 6.49 (s, 1H, CH-indole), 7.00 (d, 1H, $J$ = 8.0 Hz, H–Ar), 7.04 (t, 1H, $J$ = 6.8 Hz, H–Ar), 7.29 (s, 1H, H–Ar). 7.30–7.45 (m, 9H, H–Ar). 7.67–7.72 (m, 3H, H–Ar), 7.78–7.80 (m, 2H, H–Ar), 7.86 (dd, 1H, $J$ = 1.2 and 8.0 Hz, H–Ar), 12.97 (s, 1H, OH). $^{13}$C NMR (101 MHz, DMSO-$d_6$): $\delta$ = 43.42, 60.44, 95.33, 106.84, 110.46, 115.51, 116.83, 121.65, 123.49, 123.92, 124.02, 124.99, 125.09, 125.12, 127.48, 127.89, 127.99, 128.86, 129.14, 130.49, 131.77, 132.63, 133.72, 136.13, 140.34, 143.50, 145.79, 148.25, 152.56, 160.10, 163.63, 171.95. Anal. calcd for $C_{33}H_{22}BrN_3O_4$ (603.07): C, 65.57; H, 3.67; N, 6.95. Found: C, 65.70; H, 3.84; N, 7.12.

*4.1.1.23 3-(5-(4-Bromophenyl)-3-(4-hydroxy-2-oxo-2H-chromen-3-yl)-1H-pyrazol-1-yl)-5-chloroindolin-2-one* ***6d***. White powder, m.p. > 300 °C, yield (0.42 g, 77%). $^1$H NMR (400 MHz, DMSO-$d_6$): $\delta$ = 6.26 (s, 1H, CH-indole), 6.92 (d, 1H, $J$ = 8.8 Hz, H–Ar), 7.24 (s, 1H, H–Ar), 7.36–7.44 (m, 3H, H–Ar), 7.52–7.55 (m, 2H, H–Ar), 7.66–7.69 (m, 2H, H–Ar), 7.77 (d, 2H, $J$ = 8.4 Hz, H–Ar), 7.87–7.89 (m, 1H, H–Ar), 11.00 (s, 1H, NH), 13.09 (s, 1H, OH). $^{13}$C NMR (101 MHz, DMSO-$d_6$): $\delta$ = 60.69, 95.26, 106.46, 114.34, 115.38, 116.52, 123.88, 124.12, 124.90, 127.89, 128.03, 128.24, 131.83, 132.17, 132.52, 133.18, 133.71, 142.54, 148.15, 152.44, 160.01, 163.58, 173.00. Anal. calcd for $C_{26}H_{15}BrClN_3O_4$ (548.77): C, 56.90; H, 2.76; N, 7.66. Found: C, 57.01; H, 2.92; N, 7.79.

*4.1.1.24 3-(5-(4-Bromophenyl)-3-(4-hydroxy-2-oxo-2H-chromen-3-yl)-1H-pyrazol-1-yl)-5-chloro-1-ethylindolin-2-one* ***6e***. Off-white powder, m.p. 275–277 °C, yield (0.44 g, 76%). $^1$H NMR (400 MHz, DMSO-$d_6$): $\delta$ = 1.10 (t, 3H, $J$ = 7.2 Hz, $CH_3$), 3.68 (q, 2H, $J$ = 6.8 Hz, $CH_2$), 6.30 (s, 1H, CH-indole), 7.20–7.22 (m, 2H, H–Ar). 7.31–7.35 (m, 1H, H–Ar), 7.37–7.39 (m, 1H, H–Ar), 7.44–7.48 (m, 2H, H–Ar), 7.57–7.66 (m, 3H, H–Ar), 7.72 (d, 2H, $J$ = 8.8 Hz, H–Ar), 7.82 (dd, 1H, $J$ = 1.2 and 8.0 Hz, H–Ar), 12.97 (s, 1H, OH). $^{13}$C NMR (101 MHz, DMSO-$d_6$): $\delta$ = 12.65, 35.17, 60.27, 69.51, 95.35, 106.89, 111.32, 115.41, 116.77, 123.88, 124.08, 124.87, 125.45, 127.09, 127.30, 127.79, 130.38, 131.82, 132.46, 133.68, 142.40, 145.61, 148.15, 152.48, 160.04, 163.56, 170.94. Anal. calcd for $C_{28}H_{19}BrClN_3O_4$ (576.82): C, 58.30; H, 3.32; N, 7.28. Found: C, 58.48; H, 3.50; N, 7.44.

*4.1.1.25 1-Benzyl-3-(5-(4-bromophenyl)-3-(4-hydroxy-2-oxo-2H-chromen-3-yl)-1H-pyrazol-1-yl)-5-chloroindolin-2-one* ***6f***. Violet crystals, m.p. 222–223 °C, yield (0.42 g, 66%). $^1$H NMR (400 MHz, DMSO-$d_6$): $\delta$ = 4.91 (d, 1H, $J$ = 16.0 Hz, $CH_a$-benzyl), 5.03 (d, 1H, $J$ = 16.00 Hz, $CH_b$-benzyl), 6.49 (s, 1H, CH-indole), 7.02

(d, 1H, $J$ = 8.4 Hz, H–Ar), 7.29 (s, 1H, H–Ar), 7.34–7.45 (m, 8H, H–Ar), 7.53–7.54 (m, 1H, H–Ar), 7.67–7.74 (m, 3H, H–Ar), 7.79–7.81 (m, 2H, H–Ar), 7.88 (dd, 1H, $J$ = 1.2 and 7.6 Hz, H–Ar), 12.96 (s, 1H, OH). $^{13}$C NMR (101 MHz, DMSO-$d_6$): $\delta$ = 43.49, 60.21, 95.35, 106.89, 111.90, 115.47, 116.83, 123.97, 124.06, 125.00, 125.54, 127.02, 127.44, 127.64, 127.85, 128.06, 129.18, 129.68, 130.35, 131.90, 132.59, 133.75, 135.82, 142.50, 146.04, 148.46, 152.56, 160.08, 163.65, 171.71. Anal. calcd for $C_{33}H_{21}BrClN_3O_4$ (637.04): C, 62.04; H, 3.31; N, 6.58. Found: C, 62.22; H, 3.51; N, 6.77.

*4.1.1.26 5-Bromo-3-(5-(4-bromophenyl)-3-(4-hydroxy-2-oxo-2H-chromen-3-yl)-1H-pyrazol-1-yl) indolin-2-one* ***6g***. Off-white powder, m.p. 298–299 °C, yield (0.36 g, 60%). $^1$H NMR (400 MHz, DMSO-$d_6$): $\delta$ = 6.27 (s, 1H, CH-indole), 6.97 (d, 1H, $J$ = 8.4 Hz, H–Ar), 7.25 (s, 1H, H–Ar), 7.36–7.44 (m, 4H, H–Ar), 7.66–7.70 (m, 3H, H–Ar), 7.77 (d, 2H, $J$ = 8.4 Hz, H–Ar), 7.87 (dd, 1H, $J$ = 1.2 and 8.0 Hz, H–Ar), 10.99 (s, 1H, NH), 13.09 (s, 1H, OH). $^{13}$C NMR (101 MHz, DMSO-$d_6$): $\delta$ = 60.74, 95.39, 106.75, 112.19, 115.48, 116.81, 123.89, 124.12, 124.91, 125.59, 126.70, 127.67, 127.89, 130.38, 131.83, 132.53, 133.72, 142.10, 145.75, 148.15, 152.54, 160.08, 163.62, 173.05. Anal. calcd. For $C_{26}H_{15}Br_2N_3O_4$ (593.22): C, 52.64; H, 2.55; N, 7.08. Found: C, 52.75; H, 2.69; N, 7.22.

*4.1.1.27 5-Bromo-3-(5-(4-bromophenyl)-3-(4-hydroxy-2-oxo-2H-chromen-3-yl)-1H-pyrazol-1-yl)-1-ethylindolin-2-one* ***6h***. Buff powder, m.p. 276–278 °C, yield (0.41 g, 66%). $^1$H NMR (400 MHz, DMSO-$d_6$): $\delta$ = 1.14 (t, 3H, $J$ = 7.2 Hz, $CH_3$), 3.66 (q, 2H, $J$ = 4.8 Hz, $CH_2$), 6.34 (s, 1H, CH-indole), 7.16–7.29 (m, 1H, H–Ar). 7.39–7.44 (m, 3H, H–Ar), 7.54–7.59 (m, 2H, H–Ar), 7.62–7.70 (m, 3H, H–Ar), 7.87 (d, 2H, $J$ = 8.4 Hz, H–Ar), 7.98 (dd, 1H, $J$ = 1.2 and 7.6 Hz, H–Ar), 12.97 (s, 1H, OH). $^{13}$C NMR (101 MHz, DMSO-$d_6$): $\delta$ = 12.60, 34.83, 95.17, 102.50, 116.45, 116.75, 120.77, 124.13, 124.70, 125.98, 127.13, 127.48, 127.92, 128.04, 129.52, 129.57, 129.64, 131.65, 133.26, 133.89, 140.20, 142.69, 148.02, 152.58, 156.48, 160.51, 164.54, 171.13. Anal. calcd for $C_{28}H_{19}Br_2N_3O_4$ (618.97): C, 54.13; H, 3.08; N, 6.76. Found: C, 54.29; H, 3.22; N, 6.92.

*4.1.1.28 1-Benzyl-5-bromo-3-(5-(4-bromophenyl)-3-(4-hydroxy-2-oxo-2H-chromen-3-yl)-1H-pyrazol-1-yl)indolin-2-one* ***6i***. Violet crystals, m.p. 218–220 °C, yield (0.44 g, 64%). $^1$H NMR (400 MHz, DMSO-$d_6$): $\delta$ = 4.73 (d, 1H, $J$ = 16.0 Hz, CH-benzyl), 4.86 (d, 1H, $J$ = 16.0 Hz, CH-benzyl), 6.32 (s, 1H, CH-indole), 6.80 (d, 1H, $J$ = 8.4 Hz, H–Ar), 7.12 (s, 1H, H–Ar), 7.14–7.27 (m, 7H, H–Ar), 7.38 (d, 1H, $J$ = 8.4 Hz, H–Ar), 7.48–7.54 (m, 4H, H–Ar), 7.62–7.64 (m, 2H, H–Ar), 7.71 (d, 1H, $J$ = 6.8 Hz, H–Ar), 12.81 (s, 1H, OH). $^{13}$C NMR (101 MHz, DMSO-$d_6$): $\delta$ = 43.46, 60.11, 95.35, 106.93, 112.38, 115.32, 115.46, 116.82, 124.05, 124.99, 127.34, 127.43, 127.49, 128.06, 128.19, 129.18, 129.65, 131.55, 131.68, 133.21, 133.74, 135.22, 135.78, 142.92, 145.98, 148.44, 152.55, 160.08, 163.64, 171.61, Anal. calcd for $C_{33}H_{21}Br_2N_3O_4$ (683.34): C, 58.00; H, 3.10; N, 6.15. Found: C, 58.17; H, 3.25; N, 6.33.

*4.1.1.29 3-(5-(4-Bromophenyl)-3-(4-hydroxy-2-oxo-2H-chromen-3-yl)-1H-pyrazol-1-yl)-5-(trifluoromethoxy)indolin-2-one* ***6j***. Yellow crystals, m.p. 298–300 °C, yield (0.46 g, 77%). $^1$H NMR (400 MHz, DMSO-$d_6$): $\delta$ = 7.06 (d, 1H, $J$ = 8.4 Hz, H–Ar), 7.25–7.28 (m, 3H, H–Ar), 7.46–7.49 (m, 1H, H–Ar), 7.59–7.69 (m, 4H, H–Ar), 7.78–7.82 (m, 3H, H–Ar), 7.84 (dd, 1H, $J$ = 1.6 and 8.0 Hz, H–Ar), 10.89 (s, 1H, NH), 13.03 (s, 1H, OH). $^{13}$C NMR (101 MHz, DMSO-$d_6$): $\delta$ = 69.95, 89.80, 92.82, 112.45, 116.68, 119.29, 120.03, 120.69, 121.83, 124.09, 125.86, 125.98, 126.14, 129.63, 130.90, 132.44, 132.59, 134.40, 141.34, 144.23, 153.38, 156.54, 163.38, 174.13. Anal. calcd for $C_{27}H_{15}BrF_3N_3O_5$ (598.32): C, 54.20; H, 2.53; N, 7.02. Found: C, 54.39; H, 2.71; N, 7.17.

### 4.2. Biology

**4.2.1. Cell lines and culture conditions.** The human melanoma cell line (A375) and normal human skin cell fibroblast cells (HSF) were obtained from Nawah Scientific Inc. (Mokattam, Cairo, Egypt) and cultured in DMEM (Dulbecco's modified Eagle's medium), Gibco, USA, supplemented with fetal bovine serum (FBS) at a concentration of 10% and 100 U mL$^{-1}$ of penicillin and streptomycin (PS). The cells were incubated at 37 °C in a humidified environment containing 5% $CO_2$.[61]

**4.2.2. Assessment of cytotoxicity by SRB assay.** Cells were seeded in 96-well plates as aliquots of 100 μL cell suspension and incubated in complete medium for 24 h. Afterward, the cells were treated with all the synthesized derivatives **4a–j**, **5a–j**, and **6a–j** (from 0.01 μM to 100 μM) for 72 h. Then, the cells were fixed for one hour at 4 °C with 150 μL of 10% trichloroacetic acid (TCA). After washing the cells five times with distilled water, 70 μL of sulforhodamine (SRB) solution (0.4% w/v) was added and incubated for 10 min at room temperature in the dark. The cells were washed with 1% acetic acid three times and allowed to air-dry. Then, 150 μL of Tris pH 10.5 (10 mM) was added, and the absorbance was measured at 540 nm. The dose–response curves of the derivatives were analyzed by applying the Emax model using the Sigma plot software. The half-maximum inhibitory concentrations ($IC_{50}$) values are reported as mean ± SD. The selectivity index (SI), which denotes the cytotoxic selectivity for the proposed treatments, was determined as SI=$IC_{50}$ of normal cells/$IC_{50}$ of tumor cells.[62]

**4.2.3. BRAF$^{V600E}$ and VEGFR-2 inhibition assay.** Aliquots of 100 μL cell suspension ($5 \times 10^3$ cells) were seeded in 96-well plates and incubated in complete media for 24 h. The cells were treated with another aliquot of 100 μL media containing 10 μM of the most potent derivative **4j**. After drug exposure for 24 h, the media were collected for the measurement of the concentrations of BRAF$^{V600E}$ and VEGFR-2 using the Human BRAF (B-Raf Proto Oncogene Serine/Threonine Protein Kinase) ELISA Kit (Elabscience) and Human VEGFR-2/KDR (vascular endothelial growth factor receptor 2) ELISA Kit (Elabscience), respectively, according to the instructions. The absorbance was measured at 450 nm using an Infinite F50 microplate reader (TECAN, Switzerland). Data are presented as percentage inhibition. The experiment was carried out at various concentrations (0.1, 0.5, 1, 5, and 10 μM) to determine the $IC_{50}$ of BRAF and VEGFR2 for derivative **4j** and sorafenib.[63]

**4.2.4. Cell cycle analysis.** Melanoma cells (A375) were seeded with $1 \times 10^5$ cells per well in a 6-well plate, incubated for 24 h, and treated with derivative **4j** and sorafenib for 48 h. Then, adherent and floating cells were collected from the cultures, washed twice with PBS (phosphate buffered saline), fixed in ice-cold 60% ethanol at 40 °C, and re-washed in PBS. Subsequently,

the cells were resuspended in 500 μL propidium iodide (PI) with RNase staining buffer, BD (Franklin Lakes, NJ, USA), and incubated for 30 min. Lastly, FACS analyses were performed utilizing an ACEA Novocyte™ flow cytometer (ACEA Biosciences Inc., San Diego, USA). For every sample, the data from 12 000 cells were collected and the distribution of cell cycle phases was analyzed using the ACEA Novo Express™ software (ACEA Biosciences Inc., San Diego, USA).[64]

**4.2.5. Apoptosis assay.** Apoptosis detection was done through a flow cytometer using the Annexin V-FITC/PI Apoptosis Detection Kit (BD Biosciences, San Diego, USA) following the manufacturer's instructions to differentiate among living, apoptotic, and necrotic cells. With a seeding density of $1 \times 10^5$ cells per well on a 6-well plate, A375 cells were treated with the $IC_{50}$ of derivative **4j** and sorafenib for 48 h. Adherent and floating cells were collected from the cultures, resuspended in 0.5 mL of binding buffer, and then staining solution. Annexin V-FITC (5 μL) and PI (5 μL) were added for 15 min at room temperature in the dark. Finally, the cells were subjected within one hour of staining to FACS analysis using an ACEA Novocyte™ flow cytometer (ACEA Biosciences Inc., San Diego, CA, USA).[65]

**4.2.6. Scratch wound healing assay (cell migration assay).** A375 cells were grown in 6-well culture plates at a seeding density of $1 \times 10^5$/well to achieve the confluent monolayer. Then, the cell monolayer was gently scratched with a sterile 200 μL pipette tip to make one straight cell-free line. After washing with PBS, the cells were treated with **4j** and sorafenib. Scratch healing was recorded at 0, 24, 48, and 72 h. The scratch images were captured at a magnification of ×100 using an inverted microscope (Olympus, Japan). The horizontal distance of the wound gap was measured using Image J (version 1.53C, NIH, US) and the percentage of wound closure calculated according to the following equation: $\%\text{Wound closure} = 100 - [(W_t/W_0) \times 100]$, where $W_t$ is the wound width at time $t$ and $W_0$ is its initial width.[66]

**4.2.7. Data analysis.** All data are presented as mean ± SD ($n = 3$). Analysis of variance (ANOVA) with Tukey's post-hoc test ($P < 0.05$) was applied using GraphPad Prism Software version 6.

### 4.3. Molecular modeling

The molecular docking studies were conducted using the Molecular Operating Environment (MOE 2022.02)[67] package license purchased from Chemical Computing Group Inc. and a Sherbrooke St, Montreal, QC, Canada. Triangle matcher was used as a placement method. The London $\Delta G$ scoring method was applied to estimate the free energy of binding (kcal $mol^{-1}$). Validation of docking was done by computing (GBVI/WSA) dG, which is a force field-based scoring function to estimate the free energy of binding (kcal $mol^{-1}$). Redocking of the co-crystalized ligand SB-5902885 was done as a type of validation as well. The root mean square deviation (RMSD) of the docked ligands was computed to measure the deviation from the co-crystalized ligand. The crystal structures of BRAF (**PBD = 2FB8**) and VEGFR-2 (**PBD = 3VO3**) were downloaded from the Protein Data Bank (**https://www.rcsb.org**).

### 4.4. ADME prediction

ADME prediction of all pharmacokinetic properties was performed and validated using two platforms, *i.e.* ADMETLab 2.0 [68] and pKCSM.[69]

## Ethical approval

This study was conducted according to the appropriate ethical standards as required by guidance from The Medical Research Ethics Committee (MREC), Egypt, Ethical Clearance Certificate No. 9446072023.

## Conflicts of interest

There are no conflicts of interest to declare.

## References

1 G. C. Leonardi, L. Falzone, R. Salemi, A. Zanghì, D. A. Spandidos, J. A. Mccubrey, S. Candido and M. Libra, Cutaneous melanoma: from pathogenesis to therapy (Review), *Int. J. Oncol.*, 2018, **52**, 1071–1080.
2 B. A. Shoo and M. Kashani-Sabet, Melanoma arising in African-, Asian-, Latino- and Native-American populations, *Semin. Cutaneous Med. Surg.*, 2009, **28**, 96–102.
3 V. Lai, W. Cranwell and R. Sinclair, Epidemiology of skin cancer in the mature patient, *Clin. Dermatol.*, 2018, **36**, 167–176.
4 T. Amaral, T. Sinnberg, F. Meier, C. Krepler, M. Levesque, H. Niessner and C. Garbe, The mitogen-activated protein kinase pathway in melanoma part I - Activation and primary resistance mechanisms to BRAF inhibition, *Eur. J. Cancer*, 2017, **73**, 85–92.
5 G. Maurer, B. Tarkowski and M. Baccarini, Raf kinases in cancer-roles and therapeutic opportunities, *Oncogene*, 2011, **30**, 3477–3488.
6 D. T. Leicht, V. Balan, A. Kaplun, V. Singh-Gupta, L. Kaplun, M. Dobson and G. Tzivion, Raf kinases: function, regulation and role in human cancer, *Biochim. Biophys. Acta*, 2007, **1773**, 1196–1212.
7 M. A. Rahman, A. Salajegheh, R. A. Smith and A. K. Lam, B-Raf mutation: a key player in molecular biology of cancer, *Exp. Mol. Pathol.*, 2013, **95**, 336–342.
8 H. Davies, G. R. Bignell, C. Cox, P. Stephens, S. Edkins, S. Clegg, *et al.*, Mutations of the BRAF gene in human cancer, *Nature*, 2002, **417**, 949–954.
9 M. Dankner, A. A. N. Rose, S. Rajkumar, P. M. Siegel and I. R. Watson, Classifying BRAF alterations in cancer: new rational therapeutic strategies for actionable mutations, *Oncogene*, 2018, **37**, 3183–3199.
10 Y. S. Jo, S. Li, J. H. Song, K. H. Kwon, J. C. Lee, S. Y. Rha, H. J. Lee, J. Y. Sul, G. R. Kweon, H. K. Ro, J. M. Kim and M. Shong, Influence of the BRAF V600E mutation on expression of vascular endothelial growth factor in papillary thyroid cancer, *J. Clin. Endocrinol. Metab.*, 2006, **91**, 3667–3670.

11 P. A. Ascierto, J. M. Kirkwood, J. J. Grob, E. Simeone, A. M. Grimaldi, M. Maio, G. Palmieri, A. Testori, F. M. Marincola and N. Mozzillo, The role of BRAF V600 mutation in melanoma, *J. Transl. Med.*, 2012, **10**, 85.

12 S. C. Lalla, A. B. Kumar, J. S. Lehman, C. M. Lohse and J. D. Brewer, Association of BRAF V600E Status of Incident Melanoma and Risk for a Second Primary Malignancy: A Population-Based Study, *Cutis*, 2022, **110**, 150–154.

13 A. Vultur, J. Villanueva and M. Herlyn, Targeting BRAF in advanced melanoma: a first step toward manageable disease, *Clin. Cancer Res.*, 2011, **17**, 1658–1663.

14 K. Singh, P. Sonawane, A. Kumar, H. Singh, V. Naumovich, P. Pathak, M. Grishina, H. Khalilullah, M. Jaremko, A. H. Emwas, A. Verma and P. Kumar, Challenges and Opportunities in the Crusade of BRAF Inhibitors: From 2002 to 2022, *ACS Omega*, 2023, **8**, 27819–27844.

15 M. Holderfield, T. E. Nagel and D. D. Stuart, Mechanism and consequences of RAF kinase activation by small-molecule inhibitors, *Br. J. Cancer*, 2014, **111**, 640–645.

16 Y. Liu and N. S. Gray, Rational design of inhibitors that bind to inactive kinase conformations, *Nat. Chem. Biol.*, 2006, **2**, 358–364.

17 Y. Wang, S. Wan, Z. Li, Y. Fu, G. Wang, J. Zhang and X. Wu, Design, synthesis, biological evaluation and molecular modeling of novel 1H-pyrazolo[3,4-d] pyrimidine derivatives as BRAFV600E and VEGFR-2 dual inhibitors, *Eur. J. Med. Chem.*, 2018, **155**, 210–228.

18 I. H. Ali, H. T. Abdel-Mohsen, M. M. Mounier, M. T. Abo-Elfadl, A. M. El Kerdawy and I. A. Y. Ghannam, Design, synthesis and anticancer activity of novel 2-arylbenzimidazole/2-thiopyrimidines and 2-thioquinazolin-4(3H)-ones conjugates as targeted RAF and VEGFR-2 kinases inhibitors, *Bioorg. Chem.*, 2022, **126**, 105883.

19 A. Kim and M. S. Cohen, The discovery of vemurafenib for the treatment of BRAF-mutated metastatic melanoma, *Expert Opin. Drug Discovery*, 2016, **11**, 907–916.

20 R. Kainthla, K. B. Kim and G. S. Falchook, *Dabrafenib. Recent Results Cancer Res.*, 2014, **201**, 227–240.

21 P. Koelblinger, O. Thuerigen and R. Dummer, Development of encorafenib for BRAF-mutated advanced melanoma, *Curr. Opin. Oncol.*, 2018, **30**, 125–133.

22 R. M. Anforth, T. C. Blumetti, R. F. Kefford, R. Sharma, R. A. Scolyer, S. Kossard, G. V. Long and P. Fernandez-Peñas, Cutaneous manifestations of dabrafenib (GSK2118436): a selective inhibitor of mutant BRAF in patients with metastatic melanoma, *Br. J. Dermatol.*, 2012, **167**, 1153–1160.

23 G. S. Falchook, G. V. Long, R. Kurzrock, K. B. Kim, T. H. Arkenau, M. P. Brown, O. Hamid, J. R. Infante, M. Millward, A. C. Pavlick, S. J. O'Day, S. C. Blackman, C. M. Curtis, P. Lebowitz, B. Ma, D. Ouellet and R. F. Kefford, Dabrafenib in patients with melanoma, untreated brain metastases, and other solid tumours: a phase 1 dose-escalation trial, *Lancet*, 2012, **379**, 1893–1901.

24 K. T. Flaherty, I. Puzanov, K. B. Kim, A. Ribas, G. A. McArthur, J. A. Sosman, P. J. O'Dwyer, R. J. Lee, J. F. Grippo, K. Nolop and P. B. Chapman, Inhibition of mutated, activated BRAF in metastatic melanoma, *N. Engl. J. Med.*, 2010, **363**, 809–819.

25 J. Blanc, R. Geney and C. Menet, Type II kinase inhibitors: an opportunity in cancer for rational design, Anti Canc, *Agents Med. Chem.*, 2013, **13**, 731–747.

26 M. Moore, H. W. Hirte, L. Siu, A. Oza, S. J. Hotte, O. Petrenciuc, F. Cihon, C. Lathia and B. Schwartz, Phase I study to determine the safety and pharmacokinetics of the novel Raf kinase and VEGFR inhibitor BAY 43-9006, administered for 28 days on/7 days off in patients with advanced, refractory solid tumors, *Ann. Oncol.*, 2005, **16**, 1688–1694.

27 B. Izar, W. Sharfman, F. S. Hodi, D. Lawrence, K. T. Flaherty, R. Amaravadi, K. B. Kim, I. Puzanov, J. Sosman, R. Dummer, S. M. Goldinger, L. Lam, S. Kakar, Z. Tang, O. Krieter, D. F. McDermott and M. B. Atkins, A first-in-human phase I, multicenter, open-label, dose-escalation study of the oral RAF/VEGFR-2 inhibitor (RAF265) in locally advanced or metastatic melanoma independent from BRAF mutation status, *Cancer Med.*, 2017, **6**, 1904–1914.

28 S. M. Wilhelm, C. Carter, L. Tang, D. Wilkie, A. McNabola, H. Rong, C. Chen, X. Zhang, P. Vincent, M. McHugh, Y. Cao, J. Shujath, S. Gawlak, D. Eveleigh, B. Rowley, L. Liu, L. Adnane, M. Lynch, D. Auclair, I. Taylor, R. Gedrich, A. Voznesensky, B. Riedl, L. E. Post, G. Bollag and P. A. Trail, BAY 43-9006 exhibits broad spectrum oral antitumor activity and targets the RAF/MEK/ERK pathway and receptor tyrosine kinases involved in tumor progression and angiogenesis, *Cancer Res.*, 2004, **64**, 7099–7109.

29 S. M. Wilhelm, J. Dumas, L. Adnane, M. Lynch, C. A. Carter, G. Schütz, K. H. Thierauch and D. Zopf, Regorafenib (BAY 73-4506): a new oral multikinase inhibitor of angiogenic, stromal and oncogenic receptor tyrosine kinases with potent preclinical antitumor activity, *Int. J. Cancer*, 2011, **129**, 245–255.

30 T. E. Williams, S. Subramanian, J. Verhagen, C. M. McBride, A. Costales, L. Sung, W. Antonios-McCrea, M. McKenna, A. K. Louie, S. Ramurthy, B. Levine, C. M. Shafer, T. Machajewski, P. A. Renhowe, B. A. Appleton, P. Amiri, J. Chou, D. Stuart, K. Aardalen and D. Poon, Discovery of RAF265: A Potent mut-B-RAF Inhibitor for the Treatment of Metastatic Melanoma, *ACS Med. Chem. Lett.*, 2015, **6**, 961–965.

31 R. Z. Batran, E. Y. Ahmed, H. M. Awad, K. A. Ali and N. A. Abdel Latif, EGFR and PI3K/m-TOR inhibitors: design, microwave assisted synthesis and anticancer activity of thiazole-coumarin hybrids, *RSC Adv.*, 2023, **13**, 29070–29085.

32 Y. J. Jeon, J. Y. Jang, J. H. Shim, P. K. Myung and J. I. Chae, Esculetin, a Coumarin Derivative, Exhibits Anti-proliferative and Pro-apoptotic Activity in G361 Human Malignant Melanoma, *J. Cancer Prev.*, 2015, **20**, 106–112.

33 R. D. Thornes, L. Daly, G. Lynch, B. Breslin, H. Browne, H. Y. Browne, T. Corrigan, P. Daly, G. Edwards, E. Gaffney, *et al.*, Treatment with coumarin to prevent or delay

recurrence of malignant melanoma, *J. Cancer Res. Clin. Oncol.*, 1994, **120**(Suppl), S32–S34.

34 T. Aoki, I. Hyohdoh, N. Furuichi, S. Ozawa, F. Watanabe, M. Matsushita, M. Sakaitani, K. Ori, K. Takanashi, N. Harada, Y. Tomii, M. Tabo, K. Yoshinari, Y. Aoki, N. Shimma and H. Iikura, The sulfamide moiety affords higher inhibitory activity and oral bioavailability to a series of coumarin dual selective RAF/MEK inhibitors, *Bioorg. Med. Chem. Lett.*, 2013, **23**, 6223–6227.

35 S. Han, V. Zhou, S. Pan, Y. Liu, M. Hornsby, D. McMullan, H. E. Klock, J. Haugen, S. A. Lesley, N. Gray, J. Caldwell and X. J. Gu, Identification of coumarin derivatives as a novel class of allosteric MEK1 inhibitors, *Bioorg. Med. Chem. Lett.*, 2005, **15**, 5467–5473.

36 T. K. Mohamed, R. Z. Batran, S. A. Elseginy, M. M. Ali and A. E. Mahmoud, Synthesis, anticancer effect and molecular modeling of new thiazolylpyrazolyl coumarin derivatives targeting VEGFR-2 kinase and inducing cell cycle arrest and apoptosis, *Bioorg. Chem.*, 2019, **85**, 253–273.

37 R. Z. Batran, D. H. Dawood, S. A. El-Seginy, M. M. Ali, T. J. Maher, K. S. Gugnani and A. N. Rondon-Ortiz, New Coumarin Derivatives as Anti-Breast and Anti-Cervical Cancer Agents Targeting VEGFR-2 and p38α MAPK, *Arch. Pharm.*, 2017, **350**, e1700064.

38 M. A. Dickson, M. S. Gordon, G. Edelman, J. C. Bendell, R. R. Kudchadkar, P. M. LoRusso, S. H. Johnston, D. O. Clary and G. K. Schwartz, Phase I study of XL281 (BMS-908662), a potent oral RAF kinase inhibitor, in patients with advanced solid tumors, *Invest. New Drugs*, 2015, **33**, 349–356.

39 J. Zhang, T. Liu, M. Chen, F. Liu, X. Liu, J. Zhang, J. Lin and Y. Jin, Synthesis and Biological Evaluation of Indole-2-carbohydrazide Derivatives as Anticancer Agents with Anti-angiogenic and Antiproliferative Activities, *ChemMedChem*, 2018, **13**, 1181–1192.

40 M. S. Nafie and A. T. A. Boraei, Exploration of novel VEGFR2 tyrosine kinase inhibitors via design and synthesis of new alkylated indolyl-triazole Schiff bases for targeting breast cancer, *Bioorg. Chem.*, 2022, **122**, 105708.

41 M. H. Kim, M. Kim, H. Yu, H. Kim, K. H. Yoo, T. Sim and J. M. Hah, Structure based design and syntheses of amino-1H-pyrazole amide derivatives as selective Raf kinase inhibitors in melanoma cells, *Bioorg. Med. Chem.*, 2011, **19**, 1915–1923.

42 S. F. Wang, Y. L. Zhu, P. T. Zhu, J. A. Makawana, Y. L. Zhang, M. Y. Zhao, P. C. Lv and H. L. Zhu, Design, synthesis and biological evaluation of novel 5-phenyl-1H-pyrazole derivatives as potential BRAF(V600E) inhibitors, *Bioorg. Med. Chem.*, 2014, **22**, 6201–6208.

43 C. R. Wang, Z. F. Wang, L. Shi, Z. C. Wang and H. L. Zhu, Design, synthesis, and biological evaluation of pyrazole derivatives containing acetamide bond as potential BRAFV600E inhibitors, *Bioorg. Med. Chem. Lett.*, 2018, **28**, 2382–2390.

44 H. L. Li, M. M. Su, Y. J. Xu, C. Xu, Y. S. Yang and H. L. Zhu, Design and biological evaluation of novel triaryl pyrazoline derivatives with dioxane moiety for selective BRAFV600E inhibition, *Eur. J. Med. Chem.*, 2018, **155**, 725–735.

45 Y. S. Yang, B. Yang, Y. Zou, G. Li and H. L. Zhu, Design, biological evaluation and 3D QSAR studies of novel dioxin-containing triaryl pyrazoline derivatives as potential B-Raf inhibitors, *Bioorg. Med. Chem.*, 2016, **24**, 3052–3061.

46 Y. S. Yang, Q. S. Li, S. Sun, Y. B. Zhang, X. L. Wang, F. Zhang, J. F. Tang and H. L. Zhu, Design, modification and 3D QSAR studies of novel 2,3-dihydrobenzo[b][1,4]dioxin-containing 4,5-dihydro-1H-pyrazole derivatives as inhibitors of B-Raf kinase, *Bioorg. Med. Chem.*, 2012, **20**, 6048–6058.

47 R. Z. Batran, D. H. Dawood, S. A. El-Seginy, M. M. Ali, T. J. Maher, K. S. Gugnani and A. N. Rondon-Ortiz, New Coumarin Derivatives as Anti-Breast and Anti-Cervical Cancer Agents Targeting VEGFR-2 and p38α MAPK, *Arch. Pharm.*, 2017, **350**, e1700064.

48 O. M. Hafez, M. I. Nassar, S. M. El-Kousy, A. F. Abdel-Razik, M. M. Sherien and M. M. El-Ghonemy, Synthesis of some new carbonitriles and pyrazole coumarin derivatives with potent antitumor and antimicrobial activities, *Acta Pol. Pharm.*, 2014, **71**, 594–601.

49 H. S. Anbar, M. I. El-Gamal, H. Tarazi, B. S. Lee, H. R. Jeon, D. Kwon and C. H. Oh, Imidazothiazole-based potent inhibitors of V600E-B-RAF kinase with promising anti-melanoma activity: biological and computational studies, *J. Enzyme Inhib. Med. Chem.*, 2020, **35**, 1712–1726.

50 M. Koley, J. Han, V. A. Soloshonok, S. Mojumder, R. Javahershenas and A. Makarem, Latest developments in coumarin-based anticancer agents: mechanism of action and structure–activity relationship studies, *RSC Med. Chem.*, 2024, **15**, 10–54.

51 T. Neamatallah, A. M. Malebari, A. J. Alamoudi, S. Nazreen, M. M. Alam, H. H. Bin-Melaih, O. A. Abuzinadah, S. M. Badr-Eldin, G. Alhassani, L. Makki and M. Z. Nasrullah, Andrographolide nanophytosomes exhibit enhanced cellular delivery and pro-apoptotic activities in HepG2 liver cancer cells, *Drug Delivery*, 2023, **30**, 2174209.

52 L. Arce-Ramos, J. C. Castillo and D. Becerra, Synthesis and Biological Studies of Benzo[b]furan Derivatives: A Review from 2011 to 2022, *Pharmaceuticals*, 2023, **16**, 1265.

53 A. A. Bahman, M. S. I. Abaza, S. I. Khoushiash and R. J. Al-Attiyah, Sequence-dependent effect of sorafenib in combination with natural phenolic compounds on hepatic cancer cells and the possible mechanism of action, *Int. J. Mol. Med.*, 2018, **42**, 1695–1715.

54 J. O. Pinho, M. Matias, A. Godinho-Santos, J. D. Amaral, E. Mendes, M. J. Perry, A. P. Francisco, C. M. P. Rodrigues and M. M. Gaspar, A step forward on the in vitro and in vivo assessment of a novel nanomedicine against melanoma, *Int. J. Pharm.*, 2023, **640**, 123011.

55 C. Rosen, T. Mayes, C. Overholt and B. Lucke-Wold, Treatment of Melanoma Metastasis: Surgical, Chemotherapy, and Innovation, *Med. Discovery*, 2023, **2**, 1032.

56 K. Palm, P. Stenberg, K. Luthman and P. Artursson, Polar molecular surface properties predict the intestinal

absorption of drugs in humans, *Pharm. Res.*, 1997, **14**, 568–571.

57 J. Kelder, P. D. Grootenhuis, D. M. Bayada, L. P. Delbressine and J. P. Ploemen, Polar molecular surface as a dominating determinant for oral absorption and brain penetration of drugs, *Pharm. Res.*, 1999, **16**, 1514–1519.

58 D. F. Veber, S. R. Johnson, H. Y. Cheng, B. R. Smith, K. W. Ward and K. D. Kopple, Molecular properties that influence the oral bioavailability of drug candidates, *J. Med. Chem.*, 2002, **45**, 2615–2623.

59 M. F. Abo-Ashour, W. M. Eldehna, A. Nocentini, A. Bonardi, S. Bua, H. S. Ibrahim, M. M. Elaasser, V. Kryštof, R. Jorda, P. Gratteri, S. M. Abou-Seri and C. T. Supuran, 3-Hydrazinoisatin-based benzenesulfonamides as novel carbonic anhydrase inhibitors endowed with anticancer activity: synthesis, in vitro biological evaluation and in silico insights, *Eur. J. Med. Chem.*, 2019, **184**, 111768.

60 W. M. Eldehna, S. T. Al-Rashood, T. Al-Warhi, R. O. Eskandrani, A. Alharbi and A. M. El Kerdawy, Novel oxindole/benzofuran hybrids as potential dual CDK2/GSK-3β inhibitors targeting breast cancer: design, synthesis, biological evaluation, and in silico studies, *J. Enzyme Inhib. Med. Chem.*, 2021, **36**, 270–285.

61 D. A. Abosedera, S. A. Emara, O. A. S. Tamam, O. M. Badr, S. A. M. Khalifa, H. R. El-Seedi and M. S. Refaey, Metabolomic profile and in vitro evaluation of the cytotoxic activity of Asphodelus microcarpus against human malignant melanoma cells A375, *Arabian J. Chem.*, 2022, **15**, 104174.

62 A. A. Hassabo, M. Abdelraof and R. M. Allam, L-arginase from Streptomyces diastaticus MAM5 as a potential therapeutic agent in breast cancer: purification, characterization, G1 phase arrest and autophagy induction, *Int. J. Biol. Macromol.*, 2023, **224**, 634–645.

63 T. Atakul, Serum Levels of Angiogenic Factors Distinguish Between Women with Preeclampsia and Normotensive Pregnant Women But Not Severity of Preeclampsia in an Obstetric Center in Turkey, *Med. Sci. Monit.*, 2019, **25**, 6935–6942.

64 O. E. Abdel-Sattar, R. M. Allam, A. M. Al-Abd, B. Avula, K. Katragunta, I. A. Khan, A. M. El-Desoky, S. O. Mohamed, A. El-Halawany, E. Abdel-Sattar and M. R. Meselhy, Cytotoxic and chemomodulatory effects of Phyllanthus niruri in MCF-7 and MCF-7ADR breast cancer cells, *Sci. Rep.*, 2023, **13**, 2683.

65 M. M. F. Ismail, T. Z. Shawer, R. S. Ibrahim, R. M. Allam and Y. A. Ammar, Novel quinoxaline-based VEGFR-2 inhibitors to halt angiogenesis, *Bioorg. Chem.*, 2023, **139**, 106735.

66 K. Shari, R. A. El Gedaily, R. M. Allam, K. M. Meselhy, A. E. Khaleel and E. Abdel-Sattar, Jatrophone: a cytotoxic macrocylic diterpene targeting PI3K/AKT/NF-κB pathway, inducing apoptosis and autophagy in resistant breast cancer cells, *BMC Complementary Med. Ther.*, 2023, **23**, 293.

67 C.C.G. Inc., *Molecular Operating Environment (MOE), 2022.02*, Chemical Computing Group Inc., Sherbooke St. West, Suite# 910, Montreal, QC, Canada.

68 G. Xiong, Z. Wu, J. Yi, L. Fu, Z. Yang, C. Hsieh, M. Yin, X. Zeng, C. Wu, A. Lu, X. Chen, T. Hou and D. Cao, ADMETlab 2.0: an integrated online platform for accurate and comprehensive predictions of ADMET properties, *Nucleic Acids Res.*, 2021, **49**, W5–W14.

69 D. E. Pires, T. L. Blundell and D. B. Ascher, pkCSM: Predicting Small-Molecule Pharmacokinetic and Toxicity Properties Using Graph-Based Signatures, *J. Med. Chem.*, 2015, **58**, 4066–4072.